PERGAMON

Journal of Structural Geology 24 (2002) 1861–1884

JOURNAL OF STRUCTURAL GEOLOGY

www.elsevier.com/locate/jstrugeo

The eastern Tonale fault zone: a 'natural laboratory' for crystal plastic deformation of quartz over a temperature range from 250 to 700 °C

Michael Stipp*, Holger Stünitz, Renée Heilbronner, Stefan M. Schmid

Department of Earth Sciences, Basel University, Bernoullistrasse 32, 4056 Basel, Switzerland

Received 30 November 2000; received in revised form 24 January 2002; accepted 26 February 2002

Abstract

Near the eastern end of the Tonale fault zone, a segment of the Periadriatic fault system in the Italian Alps, the Adamello intrusion produced a syn-kinematic contact aureole. A temperature gradient from ~250 to ~700 °C was determined across the Tonale fault zone using critical syn-kinematic mineral assemblages from the metasedimentary host rocks surrounding deformed quartz veins. Deformed quartz veins sampled along this temperature gradient display a transition from cataclasites to mylonites (frictional–viscous transition) at 280 ± 30 °C. Within the mylonites, zones characterized by different dynamic recrystallization mechanisms were defined: Bulging recrystallization (BLG) was dominant between ~280 and ~400 °C, subgrain rotation recrystallization (SGR) in the ~400–500 °C interval, and the transition to dominant grain boundary migration recrystallization (GBM) occurred at ~500 °C. The microstructures associated with the three recrystallization mechanisms and the transitions between them can be correlated with experimentally derived dislocation creep regimes. Bulk texture X-ray goniometry and computer-automated analysis of preferred [c]-axis orientations of porphyroclasts and recrystallized grains are used to quantify textural differences that correspond to the observed microstructural changes. Within the BLG- and SGR zones, porphyroclasts show predominantly single [c]-axis maxima. At the transition from the SGR- to the GBM zone, the texture of recrystallized grains indicates a change from [c]-axis girdles, diagnostic of multiple slip systems, to a single maximum in Y. Within the GBM zone, above 630 ± 30 °C, the textures also include submaxima, which are indicative of combined basal ⟨a⟩- and prism [c] slip.

Keywords: Dynamic recrystallization; Quartz; Frictional-viscous transition; Mylonites; Texture analysis

1. Introduction

Within natural shear zones, viscous deformation by dislocation creep is achieved over a wide range of temperatures and strain rates. Experimental studies have been carried out to complement theoretical concepts and to constrain the boundary conditions of dislocation creep with respect to physical parameters (temperature, differential stress, strain rate, water content). Hirth and Tullis (1992) characterized three experimental dislocation creep regimes for quartz based on mechanical data and using light and transmission electron microscopy (TEM). Microstructure diagnostics of these three experimental regimes can be compared with those observed in natural quartz samples (e.g. White, 1973, 1976, 1977; Garcia Celma, 1982; Urai et al., 1986; Jessell, 1987). The three experimentally defined dislocation creep regimes have been correlated with natural dynamic recrystallization microstructures in recent studies on natural mylonites (e.g. Dunlap et al., 1997; Stöckhert et al., 1999; Zulauf, 2001). However, a systematic study of the entire range of quartz recrystallization microstructures developed in nature for a single tectonometamorphic setting is not yet available. Furthermore, the microstructures are often overprinted by later deformation or annealing processes and the physical conditions (pressure, temperature, strain rate, differential stress, water content) during natural deformation are typically not well constrained compared with experiments. Hence, it is difficult to find a suitable 'natural laboratory'. Werling (1992), however, described such a 'natural laboratory' for studying quartz dynamic recrystallization, namely the Eastern Tonale fault zone in Northern Italy. Based on his investigations we collected a sample set from a single major shear zone in the Alps, covering a temperature range from approximately 250 °C up to 700 °C.

In this paper, we first review some aspects of dynamic recrystallization mechanisms with reference to natural deformation microstructures in quartz. Then, the tectonometamorphic setting of the investigated samples is described. We characterize the dynamic recrystallization microstructures of quartz, and the related texture development, both

* Corresponding author. Tel./fax: +41-61-2673613.
E-mail address: Michael.Stipp@unibas.ch (M. Stipp).

0191-8141/02/$ - see front matter
PII: S0191-8141(02)00035-4

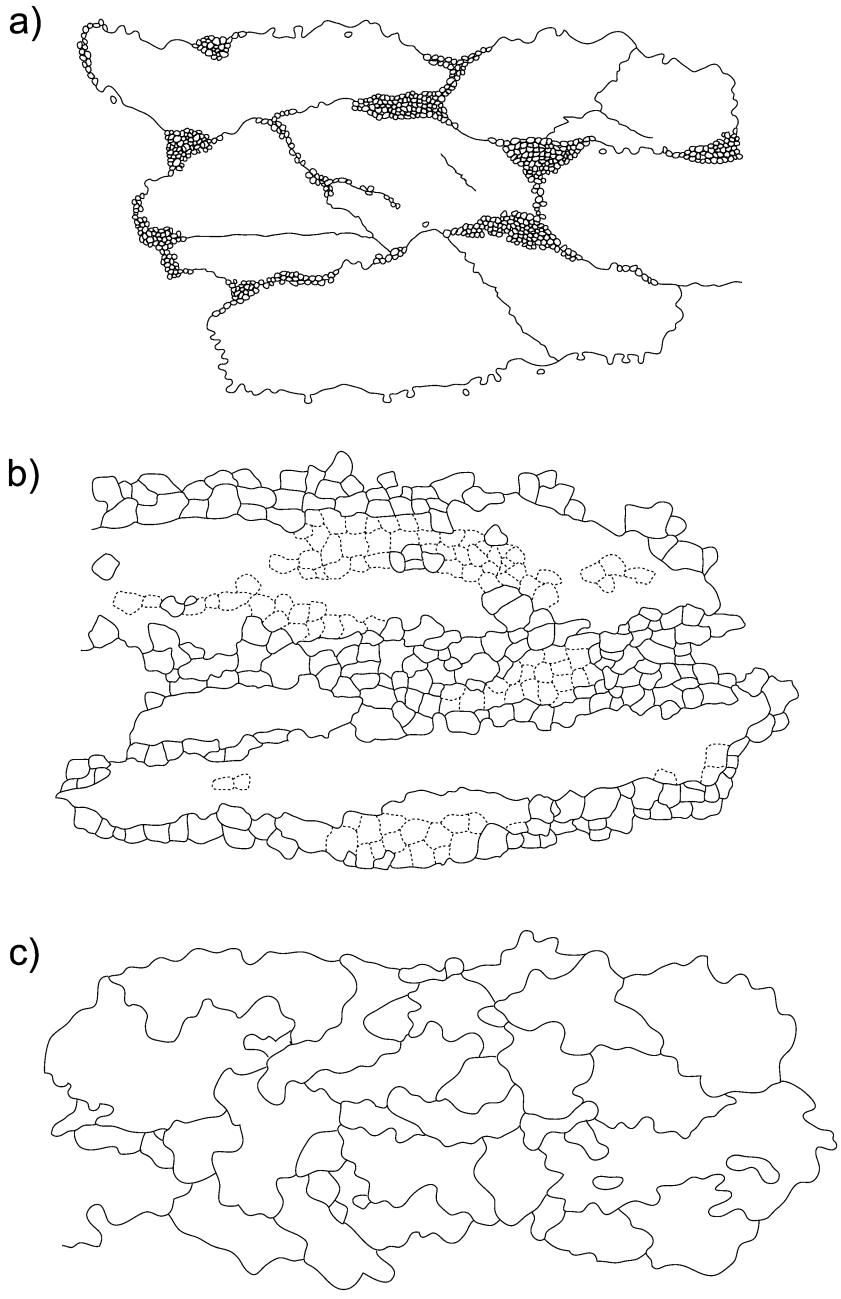

Fig. 1. Characteristic microstructures of the three dynamic recrystallization mechanisms of quartz shown at the same relative scale. (a) Bulging recrystallization (low *T*): bulges and recrystallized grains are present along grain boundaries and to a lesser extent along microcracks. (b) Subgrain rotation recrystallization (intermediate *T*): core and mantle structures of porphyroclastic ribbon grains and recrystallized subgrains. Polygonization by progressive subgrain rotation can completely consume the ribbon grains. (c) Grain boundary migration recrystallization (high *T*): irregular grain shapes and grain sizes; grain boundaries consist of interfingering sutures.

with respect to the inferred deformation temperatures. Finally, we correlate the natural microstructures with the experimental dislocation creep regimes of Hirth and Tullis (1992). This study is intended to provide criteria that may help field geologists to efficiently and quickly identify deformation microstructures in mylonitic fault zones. Therefore, we focus on light microscopy and standard methods of microfabric analysis. Furthermore, we intend to document the correlation between dominant dynamic recrystallization mechanisms and texture development over a wide temperature range of crystal plastic deformation in quartz.

2. Review of dynamic recrystallization mechanisms

Dynamic recrystallization has been defined by Poirier and Guillopé (1979) as “deformation-induced reworking of

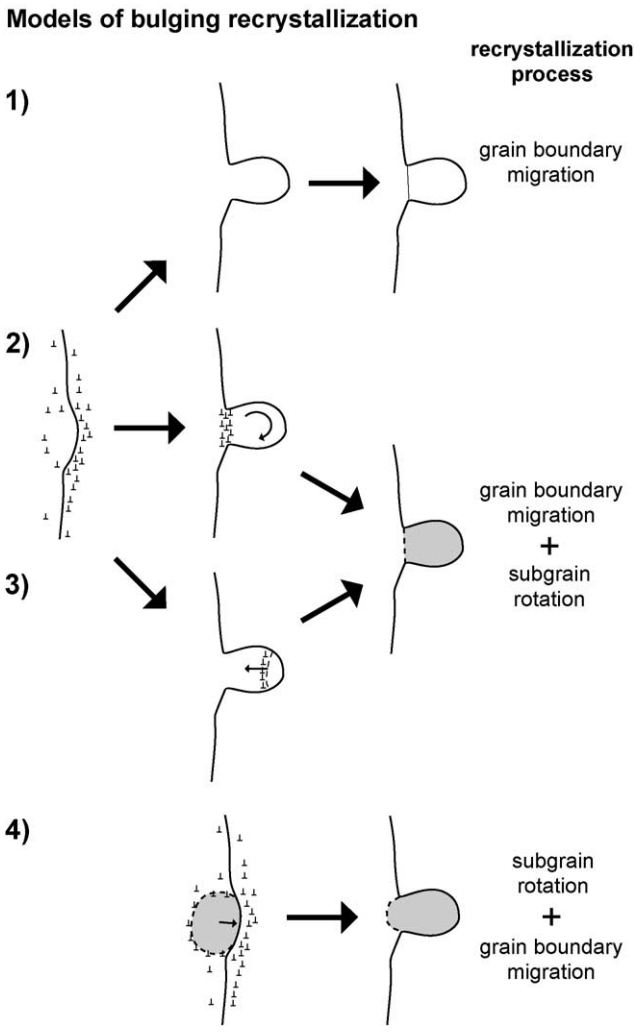

Fig. 2. Four models of the formation of new grains by bulging recrystallization; see text for explanation.

grain sizes, shapes or orientations with little or no chemical change". In quartz the mechanisms of reworking and the different recrystallization microstructures vary as a function of deformation conditions. Two distinct grain boundary processes, (1) the migration of existing grain boundaries and (2) the formation of new grain boundaries, are most important during dynamic recrystallization (e.g. White, 1977; Cahn, 1983; Drury and Urai, 1990). Two basic recrystallization processes related to these grain boundary processes have been identified: grain boundary migration (e.g. Poirier and Guillopé, 1979; Means, 1983; Poirier, 1985; Drury and Humphreys, 1986) and progressive subgrain rotation (e.g. Poirier and Nicolas, 1975; White, 1977; Guillopé and Poirier, 1979). The driving potential for subgrain rotation is the reduction of elastic distortional energy that occurs by the concentration of dislocations into walls. Strain-induced grain boundary migration is driven by differences in stored strain energy between neighboring grains (Poirier, 1985; Urai et al., 1986; Drury and Urai, 1990). Microstructures typical of subgrain rotation (e.g. Hobbs, 1968; White, 1973, 1976) and grain boundary migration recrystallization (e.g. Guillopé and Poirier, 1979; Jessell, 1987) are shown schematically in Fig. 1b and c.

These processes of subgrain rotation and grain boundary migration generally do not operate independently. Different models concerning the interaction between mechanisms of dynamic recrystallization for both metals and minerals are described by Cahn (1983), Drury et al. (1985) and Drury and Urai (1990). At lower greenschist facies conditions dynamic recrystallization of quartz occurs by localized grain boundary migration (also termed slow migration by Urai et al. (1986)), and affects only the boundary region of porphyroclasts (Fig. 1a). The resulting grain boundary bulges may be separated from the old grains, forming relatively small recrystallized grains. This type of dynamic recrystallization has been called 'bulging' by Bailey and Hirsch (1962), and we refer to it as 'bulging recrystallization' following Drury et al. (1985). Tullis and Yund (1985) demonstrate experimentally that in synthetic feldspar aggregates undergoing recrystallization-accommodated dislocation creep, grain boundaries migrate or bulge into more strained regions in the micrometre-scale and that the resulting bulges pinch off and form new, strain-free recrystallized grains. The separation of the bulges from the initial grain can involve grain boundary migration and/or subgrain rotation, which relates bulging recrystallization to the 'general recrystallization mechanisms' of Drury and Urai (1990). Different models have been proposed for bulging recrystallization (Fig. 2):

1. A strain-free bulge is developed by local slow grain-boundary migration (Bailey and Hirsch, 1962); separation of the bulge from the porphyroclast may be affected by microfracturing.
2. The bulge undergoes progressive subgrain rotation, causing a separation from the old grain by a bridging subgrain boundary (Means, 1981; Urai et al., 1986).
3. A new high-angle boundary migrates from the bulge into the old grain (Tungatt and Humphreys, 1984).
4. A subgrain at a grain boundary of a deformed grain bulges into the neighboring grain (Drury et al., 1985).

These four models illustrate some mechanisms of bulging recrystallization (BLG), producing a microstructure such as that shown in Fig. 1a. Quartz microstructures of this type have been previously referred to as regime 1 of the experimental dislocation creep regimes (Hirth and Tullis, 1992) and as marginal or low-temperature migration recrystallization microstructures in natural fault rocks (Stöckhert et al., 1999; Zulauf, 2001).

At higher temperatures subgrain rotation recrystallization (SGR; Fig. 1b) usually becomes the dominant recrystallization mechanism in natural fault rocks. At yet higher temperatures grain boundary migration recrystallization dominates (GBM; Fig. 1c). GBM is characterized by 'fast' migration (Urai et al., 1986), whereby grain boundaries

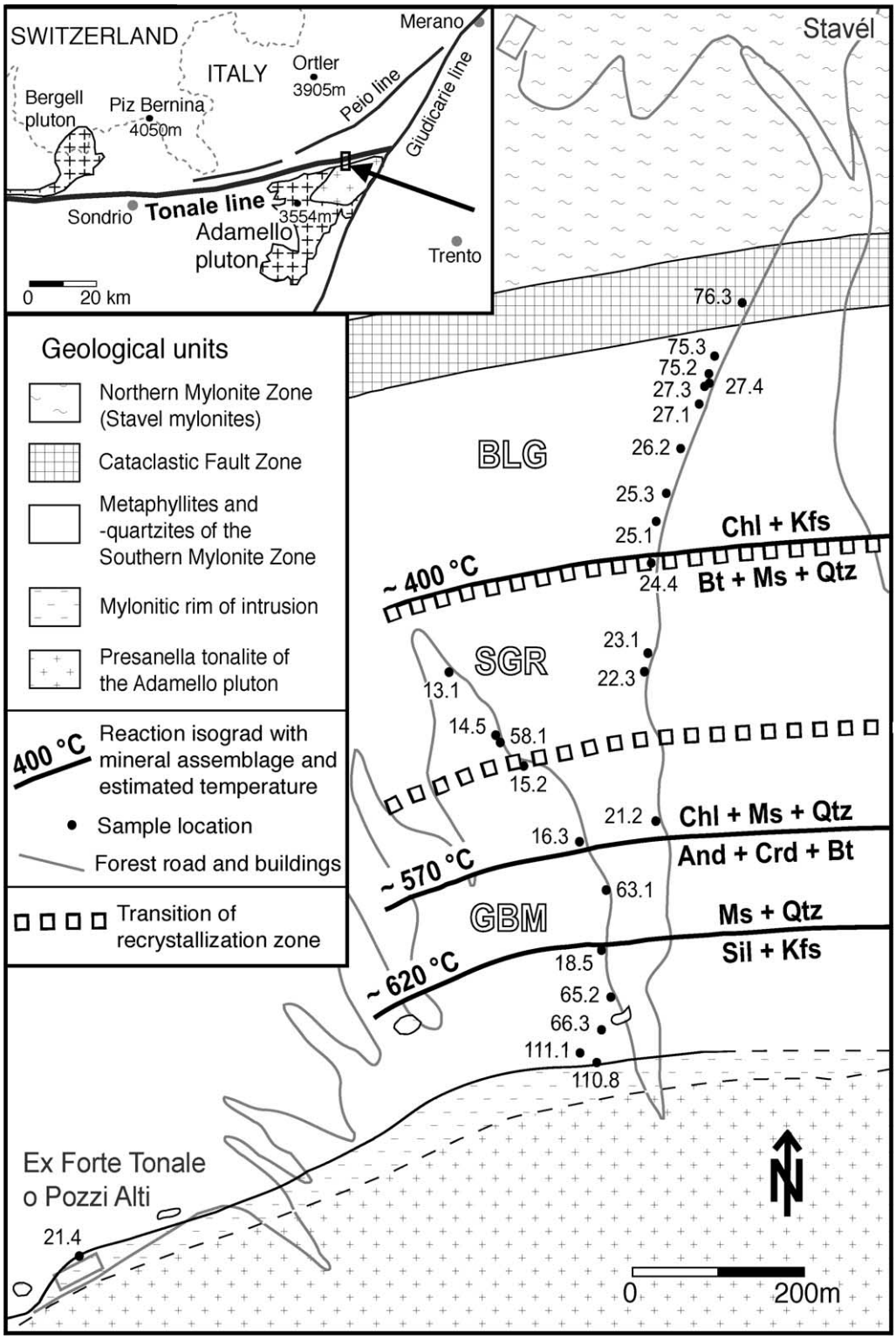

Fig. 3. Study area and location of specimens: transect across the Tonale fault zone. Temperatures of reaction isograds are inferred from mineral assemblages of metasediments (data from Werling (1992) and this study). Three dynamic recrystallization zones, BLG, SGR and GBM, are related to the metamorphic temperatures (see text). Inset: Regional (geographical and tectonic) location of study area (arrow).

Fig. 4. Mylonitic quartz vein from the Tonale line mylonites; pencil for scale.

sweep whole grains (Guillopé and Poirier, 1979). However, new grain boundaries may still form by progressive subgrain rotation. GBM can be clearly distinguished from 'slow' migration associated with bulging recrytallization (Fig. 1a). All three recrystallization mechanisms, which result from the interaction of two basic processes (i.e. subgrain rotation and grain boundary migration), can be recognized in natural dynamic recrystallization microstructures (Fig. 1). Our classification of recrystallization mechanisms operating during natural quartz deformation is comparable with that given by Urai et al. (1986). For experimentally deformed samples, Hirth and Tullis (1992) defined three dislocation creep regimes of quartz (regimes 1, 2 and 3). The identification of dislocation creep regimes is not only based on recrystallization mechanisms (although the recrystallization microstructures are an important criterion) but also on mechanical behavior. The correlation between recrystallization microstructures of naturally deformed rocks and those of the experiments is discussed in the present study. By this correlative link it is possible to extrapolate mechanical data of experimental rock deformation to the well constrained deformation conditions of the investigated natural sample set. Here, we only discuss the microstructural correlation. The mechanical extrapolation is beyond the scope of this contribution and is presented elsewhere (Stipp, 2001; Stipp et al., 2002).

3. Geological framework

3.1. Regional setting

The Tonale line, or Tonale fault zone, represents a major segment of the Periadriatic Fault System (Fig. 3; Heitzmann, 1987; Schmid et al., 1989). The eastern part of this fault zone accommodates dextral strike-slip displacements with only a small vertical component of movement (Schmid et al., 1989). The main foliation of the Tonale fault rocks is vertical and strikes E–W to ENE–WSW. A stretching lineation plunges gently (~10°) to the WSW or W.

Strike-slip displacements along the easternmost segment of the Tonale fault zone took place during a metamorphic overprint caused by the contact aureole of the Adamello pluton (Presanella unit), i.e. contact metamorphism was contemporaneous with the strike-slip movements (Martin et al., 1991; Werling, 1992; Stipp and Schmid, 1998). The study area is located in the upper Val di Sole north of the Adamello/Presanella massif (Trentino/Northern Italy; Fig. 3) and the fault rocks are exposed along a subhorizontal cross-section (Stavel profile; Fig. 3). Here, the Tonale fault zone consists of a cataclastic northern part (low temperature part of the contact aureole) and a syn-kinematic Southern Mylonite Zone (SMZ) near the intrusion (Werling, 1992). The Northern Mylonite Zone (Fig. 3), situated north of the cataclasites, is not discussed in this study because it formed earlier, i.e. before the temperature gradient was established (Stipp and Schmid, 1998).

The protolith of the SMZ consists of a series of metasedimentary rocks, which were described as contact metamorphosed Edolo schists (Trener, 1906; Mendum, 1976). Werling (1992) demonstrated that mylonitization was syn-kinematic with contact metamorphism, and determined critical mineral assemblages for a *P*/*T*-estimation. The mineral assemblages vary from chlorite-bearing lower greenschist facies parageneses in the North to sillimanite-bearing amphibolite facies parageneses in the South. Sheared quartz veins oriented parallel to the mylonitic foliation have been sampled in order to characterize the quartz dynamic recrystallization microstructures (Figs. 3 and 4).

3.2. Metamorphic conditions

The deformed rocks within the SMZ consist of a series of metapelites, metapsammites and metaquartzites. We have analyzed the mineral assemblages, considering only minerals that formed syn-kinematically in the main foliation, within pressure shadows of porphyroclasts, or along shear bands. Thus, the inferred temperatures represent deformation temperatures on the basis of reaction isograds and mineral zones (cf. Werling, 1992; Fig. 3):

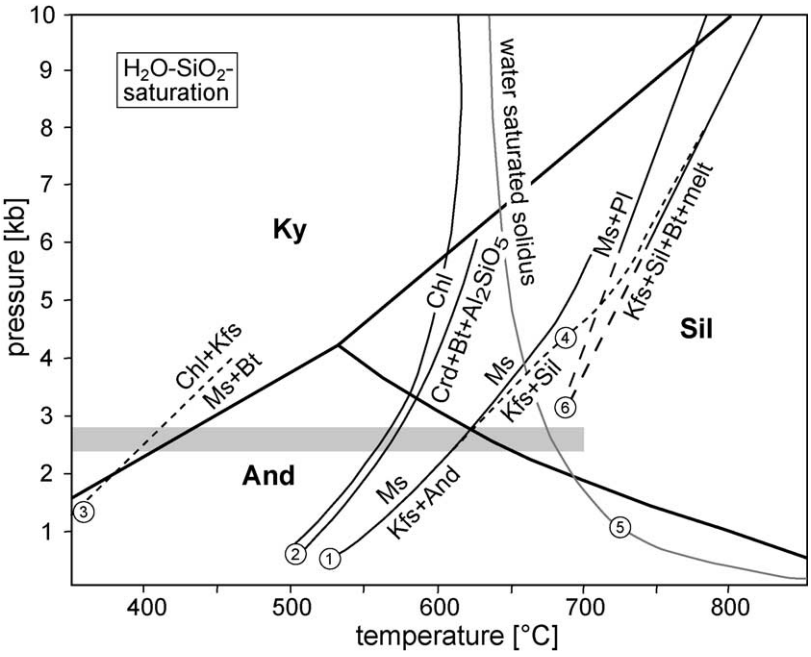

Fig. 5. Petrogenetic grid of metapelitic reactions: Al_2SiO_5 polymorphs after Kerrick (1990) and Bohlen et al. (1991). Reaction isograd (1) from Chatterjee and Johannes (1974), (2) from Spear and Cheney (1989), (3) and (4) from Bucher and Frey (1994), (5) from Johannes and Holtz (1996) and (6) from Patiño Douce and Harris (1998). Gray area represents the estimated pressure range of the Tonale line mylonites; mineral abbreviations after Kretz (1983).

The highest syn-kinematic temperatures of the contact aureole near the Presanella intrusion are inferred from the mineral reaction:

$$\text{Muscovite} + \text{Quartz} \leftrightarrow \text{K-feldspar} + Al_2SiO_5 + H_2O \quad (1)$$

and the polymorphic phase transformation:

$$\text{Andalusite} \leftrightarrow \text{Sillimanite}$$

Sillimanite formed syn-kinematically close to the magmatic contact. No syn-kinematic migmatitic microstructures could be observed and hence no melting occurred during shearing. The absence of melting confines the maximum pressure for the Kfs + Sil producing reaction to approximately 4 kb assuming a water activity $a_{H_2O} = 1$ (intersection of curves 1 and 5 in Fig. 5). A lower pressure limit of about 2 kb is given by the polymorphic transition from And to Sil (Kerrick and Heninger, 1984; Kerrick, 1990; Bohlen et al., 1991). An upper temperature limit of approximately 670 °C can be derived from the intersection of the And to Sil transition and the extrapolated dehydration melting curves of mica schists found experimentally by Patiño Douce and Harris (1998) (Fig. 5). The co-existence of Kfs and And, observed at lower temperatures further north, reduces the possible pressure range to 2.5–3 kb (Fig. 5). Since the Tonale fault zone is a strike-slip shear zone, there is no pressure gradient associated with deformation, and we infer this pressure range as representative for the whole shear zone. Given the estimated pressure range, the temperature interval for reaction isograd (1) is well defined at 620 ± 20 °C (for $a_{H_2O} = 1$; Chatterjee and Johannes, 1974; Fig. 5).

The next lower-temperature reaction isograd is defined by the mineral reaction:

$$\text{Chlorite} + \text{Muscovite} + \text{Quartz} \leftrightarrow Al_2SiO_5 + \text{Cordierite} + \text{Biotite} + H_2O \quad (2)$$

The temperature for this reaction, which produces cordierite and andalusite, is about 570 ± 20 °C for 2.5–3 kb (Spear and Cheney, 1989; Fig. 5). At temperatures below this reaction isograd, cordierite is absent but andalusite is observed with a decreasing abundance down to lower temperatures.

The lowest temperature isograd is given by the reaction:

$$\text{Chlorite} + \text{K-feldspar} \leftrightarrow \text{Muscovite} + \text{Biotite} + \text{Quartz} + H_2O \quad (3)$$

(e.g. Thompson and Norton, 1968; Pattison and Tracy, 1991). After Winkler (1979) and Yardley (1989) muscovite + biotite is stable above approximately 380 °C. Reaction (3) depends not only on temperature and pressure but also on the bulk chemistry of the rock which can be shown in a PTX_{FeO}-diagram calculated e.g. by Bucher and Frey (1994, p. 207) using the database of Holland and Powell (1990). With increasing pressure and decreasing X_{FeO} reaction isograd (3) is shifted to higher temperature. Microprobe analyses using a JEOL JXA-8600 Superprobe (15 kV acceleration voltage, 10 nA sample current and PROZA correction routine) have been carried out on samples close to reaction isograd (3) (Stipp, 2001). Based on these analyses a $X_{FeO} = 0.68 \pm 0.04$ has been determined

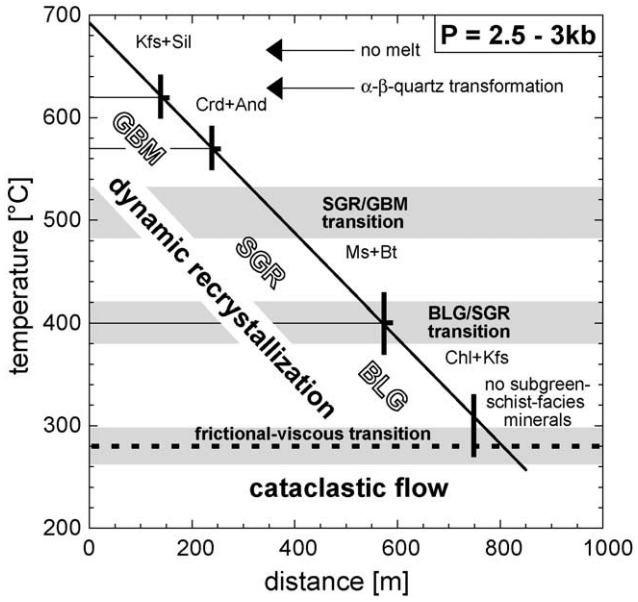

Fig. 6. Plot relating temperature to distance along the Tonale line transect. Critical mineral assemblages and zones of cataclastic flow and dynamic recrystallization of quartz are indicated. Black vertical bars are errors of temperature estimation from the reaction isograds. See text for further explanation.

for sample 24.4. The rock composition and the low confining pressure (2.5–3 kb) suggest a reaction temperature of approximately 400 ± 30 °C according to Bucher and Frey (1994).

For the lower temperature part of the cross-section it is important to distinguish between syn- and pre-kinematic biotite. Syn-kinematic biotite grains close to reaction isograd (3) are quite small, in contrast to the porphyroclastic biotite of the pre-kinematic assemblage which is decomposed to chlorite at temperatures below reaction isograd (3). The northernmost part of the SMZ contains a great amount of chlorite and no porphyroclastic biotite is present. Pre-kinematic biotite is found again in the cataclastic fault zone further north, where it was preserved metastably because of the low temperatures during cataclastic deformation. The absence of subgreenschist facies minerals in the low temperature mylonites bordering the cataclastic fault zone suggests temperatures above approximately 280–300 °C for the northern part of the SMZ (cf. Merriman and Frey, 1999).

3.3. Temperature profile across the Tonale fault zone

Using the petrologic data, deformation temperature can be plotted versus distance from the intrusion (Fig. 6): a linear trend of temperature on distance is indicated by the reaction isograds. This linear trend deviates from what is normally observed in contact metamorphism. This is probably due to the advective cooling of the aureole by the dextral strike slip movements along the Tonale fault zone (Stipp, 2001). For the transition from cataclasites (cataclastic fault zone) to mylonites (SMZ), i.e. the frictional–viscous transition (Schmid and Handy, 1991), a temperature of about 280 ± 30 °C can be inferred from the linear trend. This temperature is close to that inferred for this transition according to other studies, e.g. 300 °C (Voll, 1976), approximately 250 ± 20 °C (Dunlap et al., 1997), slightly above 310 ± 30 °C (Stöckhert et al., 1999) or approximately 270 °C (van Daalen et al., 1999). For the contact with the pluton a deformation temperature of about 700 ± 30 °C is derived. This temperature is slightly above the solidus of a water-saturated tonalite system (cf. Johannes, 1989; Johannes and Holtz, 1996). The error in temperature estimation depends on the precision of the reaction isograds in Fig. 5 and we assess the error to be ±30 °C for all inferred temperatures. The contact metamorphic setting with its related temperature gradient gives a high confidence regarding the systematic change in temperature from sample to sample.

Deformation temperatures correspond to peak temperatures reached during contact metamorphism in the investigated samples. Only in a narrow contact zone at a distance of 50–80 m from the contact was corundum found as an inclusion in andalusite and sillimanite, indicating higher peak temperatures prior to the syn-deformational assemblage (Stipp, 2001). During contact metamorphism, peak metamorphic temperatures were reached somewhat earlier in the southern part of the aureole than in the northern part. Thus, in a strict sense, the given mineral assemblages and related temperatures presented in Fig. 6 are peak temperatures that have not been attained simultaneously. The investigated syn-kinematic quartz veins of the fault zone display crystal plastic deformation of quartz ranging from approximately 250 ± 30 °C within the cataclastic fault zone to a temperature of about 670 ± 30 °C close to the magmatic contact of the Presanella intrusion.

It is important to demonstrate that mylonitic deformation was syn-kinematic with the formation of cataclasites at lower temperatures. Alternatively, the mylonites of the SMZ could have been affected by brittle deformation after decreasing temperature of the contact metamorphism. If cataclasis had overprinted earlier formed mylonites this would have left relict mylonite microstructures being incorporated as fragments within the cataclastic fault rocks. However, no fragments of mylonites were found within the cataclastic fault zone at its southern limit. Instead, the lithologies in the cataclastic zone are identical to the Edolo schist protoliths. Deformation microstructures and contact metamorphic overprint change gradually from the cataclasites into the mylonites. Hence, we conclude that the cataclastic fault rocks and the mylonites of the SMZ formed simultaneously.

3.4. Sample description

The mylonites of the Tonale fault zone display a well developed foliation and stretching lineation. Samples have

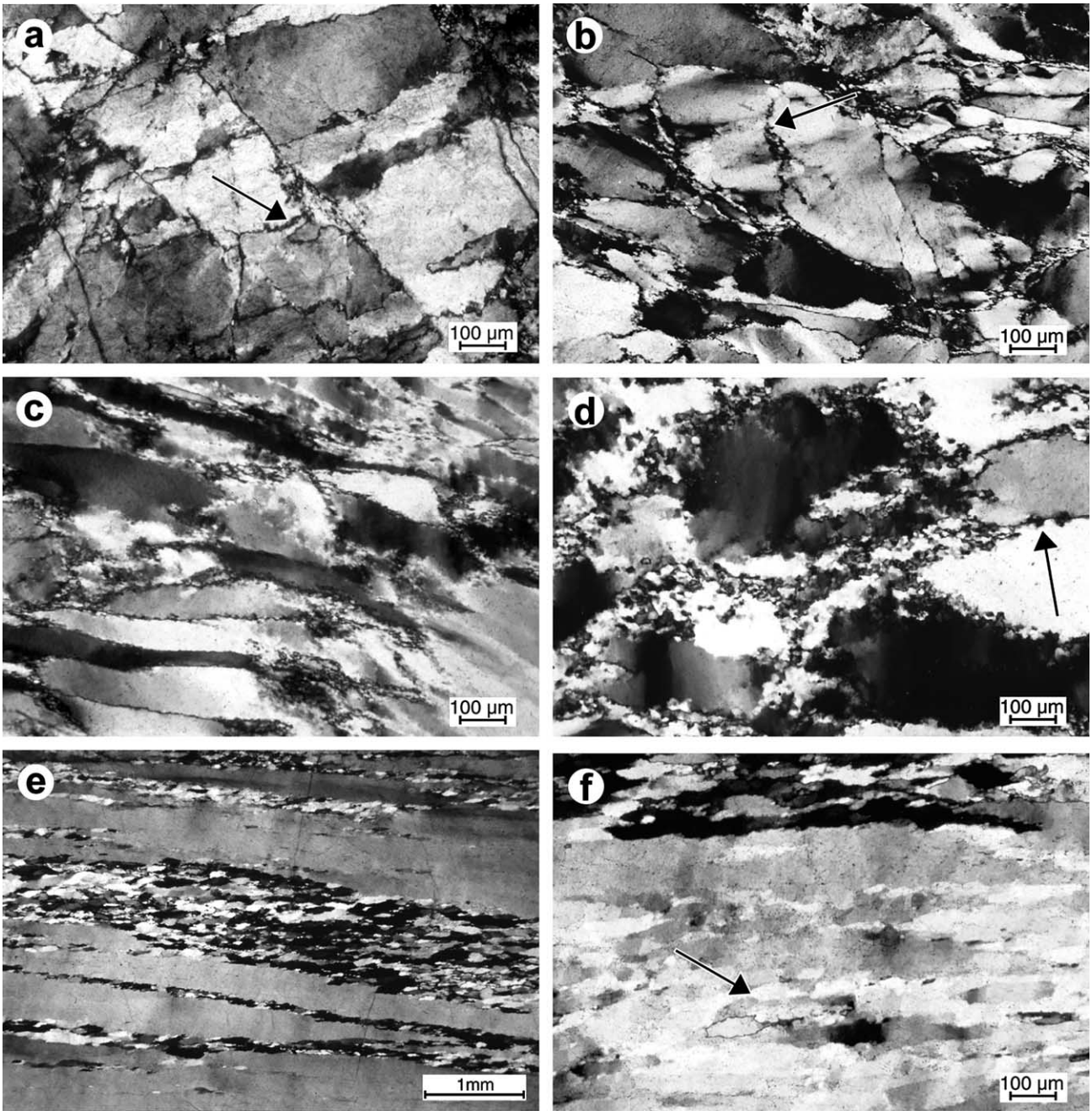

Fig. 7. Characteristic deformation microstructures of quartz veins as a function of increasing temperature: Samples were cut perpendicular to the foliation and parallel to the stretching lineation; crossed polarized light. Sample numbers correspond to locations shown in Fig. 3. (a) Cataclastic flow (~250 °C): fractured quartz from the cataclastic fault zone; sutured and serrated grain boundaries with recrystallized bulges (arrow) indicate limited crystal plasticity (sample 76.3). (b) BLG (~300 °C): Porphyroclasts with undulose and patchy extinction, serrated grain boundaries and recrystallized bulges along grain boundaries and cracks (arrow; sample 75.2). (c) BLG (~340 °C): elongated porphyroclasts with dominant bulging recrystallization, undulose and patchy extinction. Large subgrains probably pre- or postdate dynamic recrystallization (sample 26.2). (d) BLG (~400 °C): increased recrystallized grain size and volume proportion (compare with (b) and (c)); sutured grain boundaries with bulges (arrow) suggest dominant bulging recrystallization (sample 24.4). (e) SGR (~490 °C): extremely elongated ribbon grains and dominant subgrain rotation recrystallization; recrystallized grains form an oblique second foliation (sample 14.5). (f) SGR (~490 °C): polygonization due to progressive subgrain rotation; recrystallized grains (near top of figure) are about the same size as the subgrains (arrow; sample 14.5). (g) GBM (~560 °C): irregular grain shapes, sizes and boundaries due to increased grain boundary migration. Second phase particles (mainly biotite) cause pinning and reduction of the recrystallized grain size (arrows; sample 16.3). (h) GBM (~650 °C): amoeboid grains with large amplitude sutures, very large recrystallized grain sizes and dissection microstructures. Inclusions and second phase particles are small or no hindrance for inferred fast migration (sample 66.3). (i) GBM (~650 °C): chessboard extinction with subgrain boundaries parallel to prism and basal planes (sample 66.3).

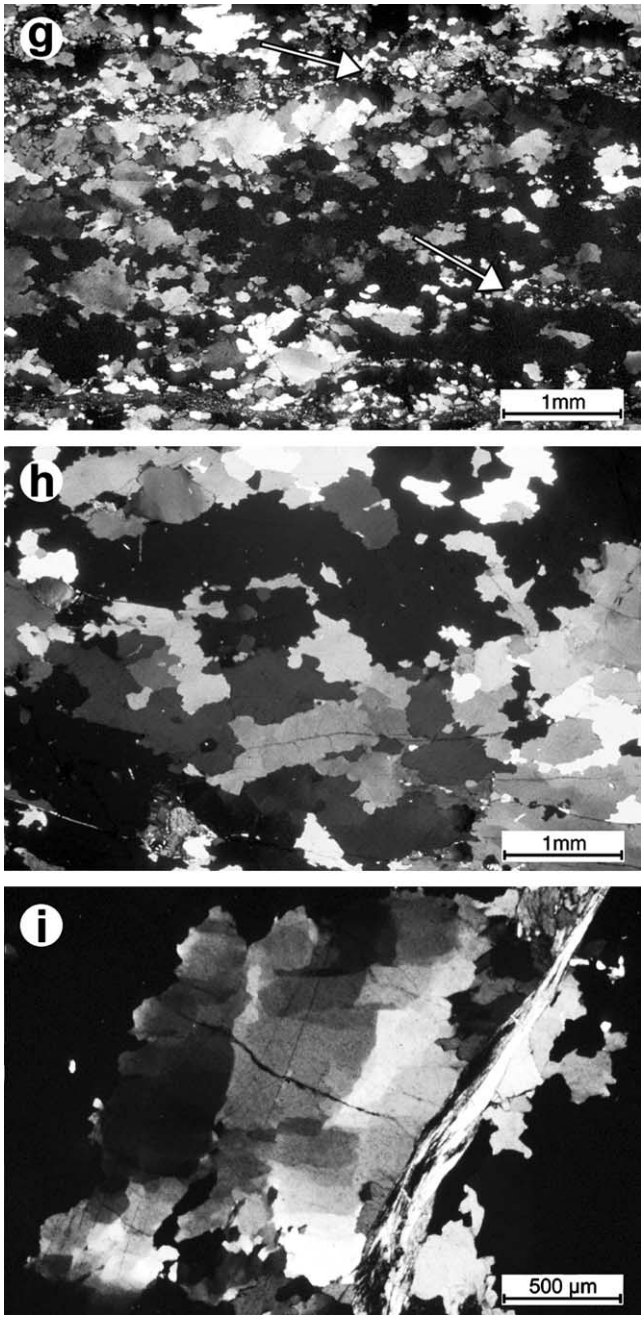

Fig. 7. (*continued*)

been analyzed in X–Z sections of the finite strain ellipsoid, i.e. normal to foliation and parallel to the stretching lineation. The sheared quartz veins used for microfabric analysis are oriented parallel to the mylonitic foliation of the metasedimentary sequence. Except for sample 21-2 (metaquartzite with a very small content of white mica) and veins from the very high temperature part of the cross-section (containing second phase particles of plagioclase, cordierite and muscovite), all investigated veins consist of pure (>99%) quartz. The thickness of the veins is in the range of less than 1 mm to about 10 cm. Veins which vary strongly in thickness have been avoided in order to ensure homogeneous strain. Within the low temperature part of the cross-section ($T < 450$ °C) wider quartz veins (>2 cm) were avoided because these usually have a lower proportion of dynamically recrystallized grains when compared with thin veins (<2 cm). In most cases, deformation appears to be concentrated in the surrounding mica- and chlorite-rich metasediments.

For every given location in the shear zone there is a prograde and retrograde path during the development of the contact aureole. As pointed out above, the deformation temperatures correspond to metamorphic peak conditions. However, later deformation during decreasing temperature conditions frequently overprint earlier formed microstructures. For this study, it is important to exclude such retrograde overprints. Therefore, the sampled quartz veins were selected on the basis of the following criteria:

1. Retrograde deformation is primarily formed in localized zones, e.g. shear bands with a very small recrystallized grain size and chloritization of biotite. Thus, these localized zones of retrogression have not been considered for the analysis.
2. To exclude more pervasive retrograde overprints (which solely occur in the higher temperature part of the aureole; $T > \sim 550$ °C) only samples with the highest temperature metamorphic mineral assemblages and the highest temperature recrystallization microstructures have been selected.
3. A few (<10) samples that do not show an unequivocal microstructure and which could not be related to the synkinematic mineral assemblage have been avoided since they may be caused by a later overprint or by inhomogeneous strain, as discussed earlier.

Only 24 out of a total set of about 120 sampled quartz veins have finally been selected. In the higher temperature part of the aureole ($T > \sim 550$ °C), all the excluded samples show clear evidence for retrogression. In the lower temperature part of the aureole some overprinted samples have also been eliminated, but the investigated samples are a representative selection from a larger number of non-overprinted samples.

4. Microstructural description

4.1. Zone of cataclastic flow

The cataclastic fault zone north of the SMZ deformed by various processes of a dominantly brittle nature (Fig. 7a). Fractures of different length occur, causing grain size reduction by fragmentation. The pre-existing fabric is more or less obliterated where the intensity of fracturing is high. Fracturing as the predominant deformation mechanism is accompanied by limited amounts of crystal plastic deformation, indicated by features such as undulose and patchy extinction (not related to microcracking), deformation

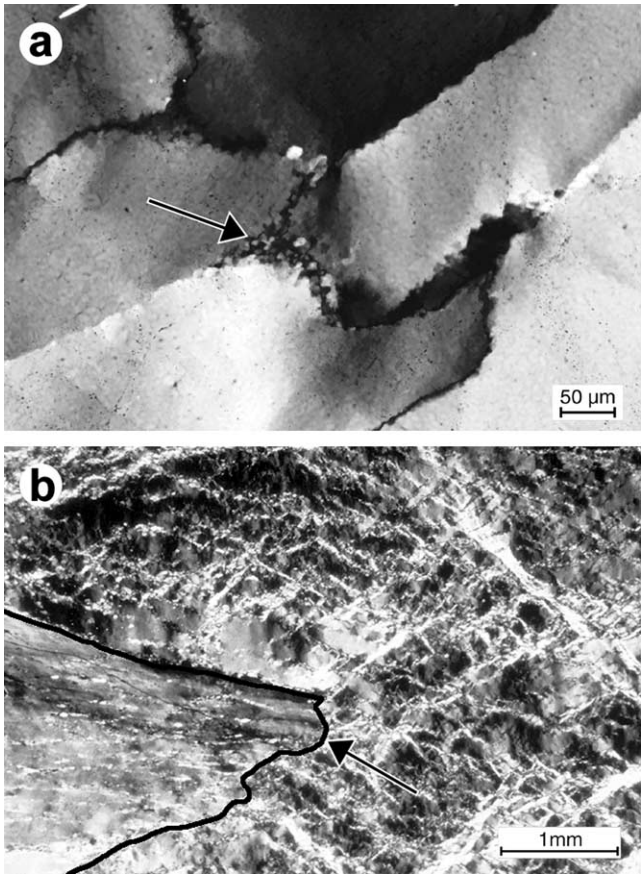

Fig. 8. Microstructural detail observations relating to bulging recrystallization: (a) BLG (~290 °C): bulges and recrystallized grains. Preferred sites of bulging are triple junctions and grain boundaries in a steep angle to the foliation (arrow); foliation trace dips ~30° to the left (sample 75.3). (b) BLG (~300 °C): intersection of two quartz fibers, one extends from the lower left corner into the other one (arrow and black outline). In the lower left quartz fiber, recrystallized grains are exceptionally well aligned parallel to the mylonitic foliation whereas the other quartz fiber displays recrystallized grains along conjugate shear band sets (sample 27.4).

bands and, locally, by sutured and serrated grain boundaries (Fig. 7a). The quartz clasts also contain subgrains. These 'subgrains' were perhaps caused by microcrack arrays, as was found in experimentally deformed feldspar (Tullis and Yund, 1985).

Some fractures can be traced into zones of small new grains (Fig. 7a). These new grains have equant shapes and small grain sizes within a narrow grain size range. Hence, these grains do not show any resemblance to cataclastic features. Instead, serrated grain boundaries and the small new grains near grain boundaries are interpreted to be the result of incipient dynamic recrystallization resulting from local grain boundary bulging and grain separation processes like those described above (bulging recrystallization; Fig. 7a). This process represents slow grain boundary migration confined to the rims of the quartz porphyroclasts or along fractures and at crack tips.

The microstructural characteristics of the cataclasites and those of the mylonites of the SMZ are transitional between

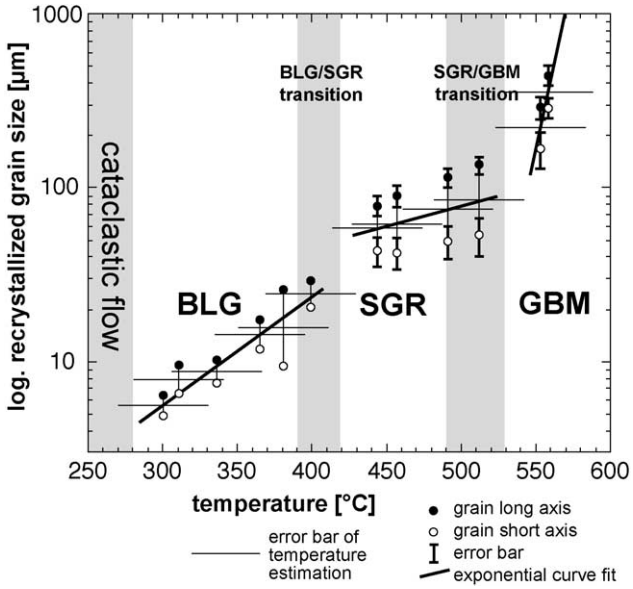

Fig. 9. Diagram of recrystallized grain size versus temperature: curve fit is based on the geometric mean of long and short grain axes.

deformation regimes. The observed deformation features within the cataclasites can be related to the regimes referred to as 'semibrittle faulting' or 'semibrittle flow' by experimentalists (e.g. Carter and Kirby, 1978; Hirth and Tullis, 1994). Obviously cataclastic and crystal plastic deformation features coexist on the microscopic scale. However, in the absence of recovery processes and widespread recrystallization near the frictional–viscous transition (cf. Schmid and Handy, 1991; Hirth and Tullis, 1994), effective pressure (hence friction) is expected to control the strength of the cataclasites. In contrast to the microscopic scale, the boundary between the cataclastic fault zone and the SMZ is quite abrupt at the outcrop scale where brittle deformation features such as fractures or cataclastic mixing of components are well visible.

4.2. Zone of bulging recrystallization (BLG)

South of the cataclastic fault zone, the investigated quartz veins consist of large quartz porphyroclasts. The latter are inhomogeneously deformed and display undulose and patchy extinction, deformation bands, deformation lamellae, kink bands, conjugate sets of shear bands (probably initiated as fractures; cf. van Daalen et al., 1999), and, locally, also large irregularly shaped subgrains (Fig. 7b). Here, the porphyroclasts appear only slightly elongated but their aspect ratio increases with temperature in the BLG zone (Fig. 7c). Small bulges were developed along old grain boundaries. New grains are also found, indicating the beginning of recrystallization by local grain boundary bulging (Fig. 8a). Preferred sites of bulging are triple junctions and old grain boundaries oriented approximately normal to the foliation. Bulging can also occur along fractures such as those described for the cataclastic fault zone

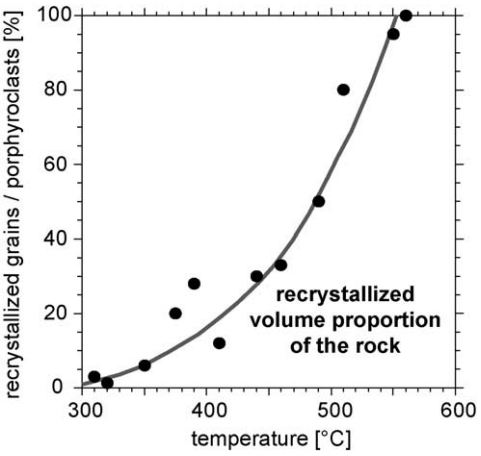

Fig. 10. Volumetric fraction of recrystallized grains as a function of the deformation temperature within BLG, SGR and beginning of GBM.

(Fig. 7b). Crosscutting fractures are much less common than in the zone of cataclastic flow, whereas intragranular microcracks are abundant. These intragranular microcracks preferentially form parallel sets with orientation variations from grain to grain suggesting that the microcrack orientation is controlled by the crystal lattice of the host grain (Vollbrecht et al., 1999). Two types of subgrains are found: (1) irregularly shaped subgrains which are much larger than the recrystallized grains and which possibly pre- or post-date dynamic recrystallization; (2) subgrains which are of the same size as the recrystallized grains and which are located at the bulged boundaries of the porphyroclasts. The latter subgrains may have formed by different processes during the bulging mechanism (Figs. 2, 7c and d and 8a). Intragranular deformation features like undulose and patchy extinction are less pronounced at higher temperature. In contrast, the fine suturation of the grain boundaries is intensified (Fig. 7d).

With increasing temperature, the size of recrystallized grains increases across the shear zone (Figs. 7b and d and 9). Recrystallized grain sizes have been determined by a combination of the line-intercept method (e.g. Etheridge and Wilkie, 1981; Ord and Christie, 1984) and image analysis techniques. A detailed description of the applied methods is given elsewhere (Stipp, 2001; Stipp et al., 2002). Grains were measured both parallel and normal to their longest axes. From the intercepts, mean long (a) and short (b) axes were calculated and the recrystallized grain size was determined from the geometric mean of short and long axes. Within the BLG zone, i.e. between 300 and 400 °C, the recrystallized grain size (mean diameter) increases from approximately 5 to 25 μm (Fig. 9). The volume proportion of recrystallized material was also determined for each sample using NIH Image (Rasband, 1996), after masking either the recrystallized or the porphyroclastic grains. The volume proportion of recrystallized material increases dramatically with increasing temperature (Fig. 10). Deviations from a best fit can be attributed to local strain heterogeneities. Within BLG, the proportion of recrystallized grains increases from 0 to 25%, leading to the formation of core and mantle structures. Thus, from these microstructures it becomes obvious that core and mantle structures are not only indicative of SGR (cf. Gifkins, 1976; White, 1976). Instead, they are also typical of the higher temperature part of BLG (cf. Fitz Gerald and Stünitz, 1993). There, a combination of limited boundary migration and subgrain rotation significantly contributes to the dynamic recrystallization.

In a few samples the porpyroclasts are very elongate. They probably represent pre-existing vein fibers which formed parallel to the vein boundaries and are parallel to the main foliation at the time of their formation (Fig. 8b). They are internally deformed and show deformation features such as crosscutting sets of conjugate shear bands. These shear bands contain new grains which may have initially formed by fracture processes, such as found by van Daalen et al. (1999) near the Glarus thrust in the Helvetic nappes.

4.3. Zone of subgrain rotation recrystallization (SGR)

Core and mantle structures typically develop at the transition from BLG to SGR (Fig. 7d). Within the SGR zone, porphyroclasts are always transformed to ribbon grains. Their shape fabric is significantly more anisotropic than that within BLG (Fig. 7e). Recrystallized grains of uniform size are arranged in layers oblique or subparallel to the main foliation (Fig. 7e). Dynamic recrystallization is dominated by progressive subgrain rotation (Fig. 7f) and is not restricted to the original grain boundary area but also affects the interior of porphyroclasts. Across the transition from BLG to SGR the recrystallized grain size increases discontinuously (Fig. 9). Within the zone of SGR, there is a slight increase of the recrystallized grain size from approximately 60 to 85 μm while the volume proportion of the recrystallized grains increases from 30 to 90% (Fig. 10). Subgrains are about the same size as the recrystallized grains (Fig. 7f) suggesting that subgrains and recrystallized grains have been formed by the same process (cf. Schmid et al., 1980; Nishikawa and Takeshita, 2000). Polygonization and subgrain rotation recrystallization produce relatively straight grain boundaries of the porphyroclasts compared with grain boundary bulging. In the light microscope, recrystallized grains show almost no intracrystalline deformation features. Intracrystalline deformation features within the ribbon grains, e.g. undulose extinction and deformation lamellae, are less common and they possibly formed during later strain increments.

Four samples from the SGR zone, corresponding to four different temperatures in the range of 440 to 510 ± 30 °C, were selected for fabric analysis. Photomicrographs of X–Z and Y–Z sections were taken with crossed polarizers. Several hundred grain boundary outlines were digitized for each sample using all optically visible grain boundaries.

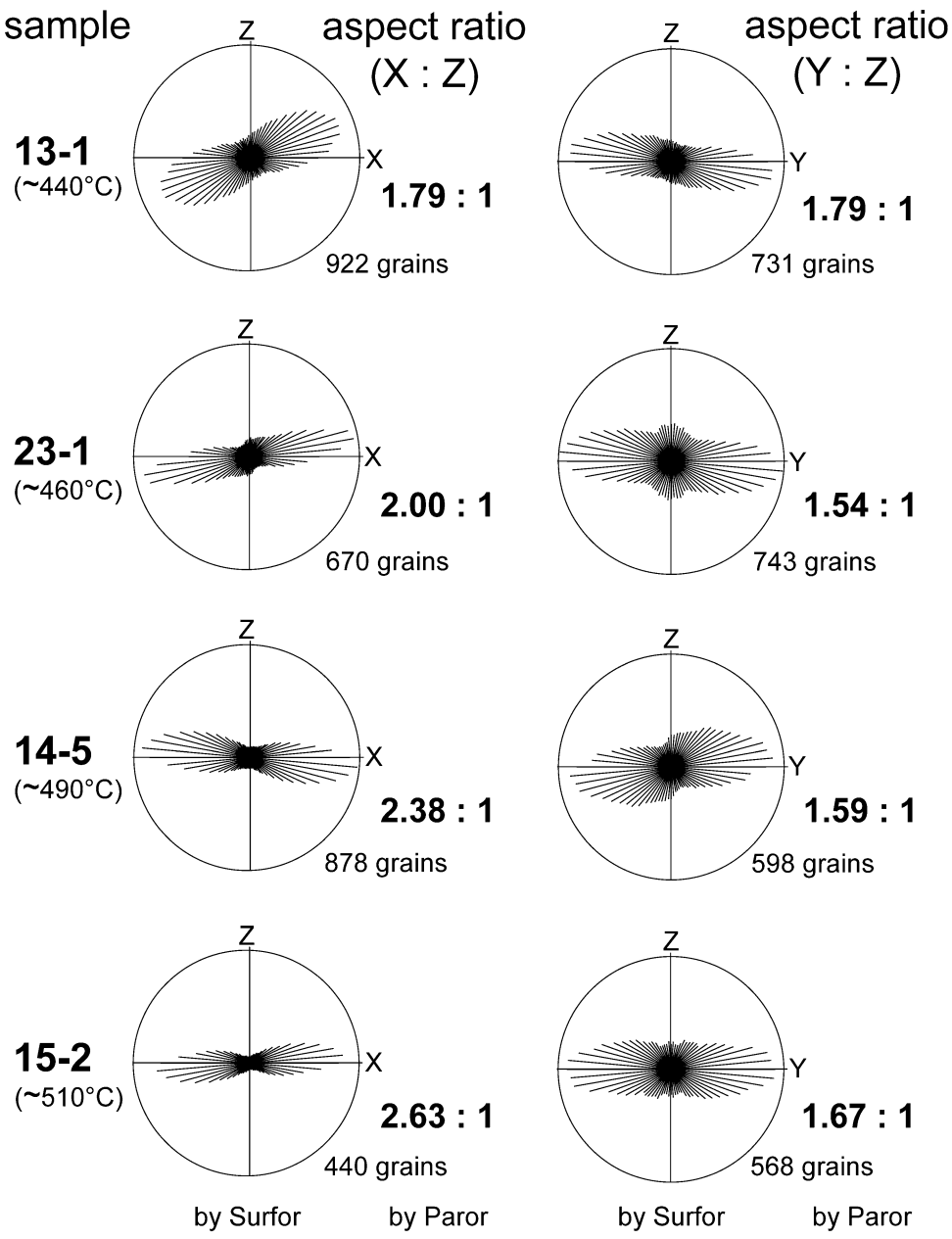

Fig. 11. Microstructural analyses of samples from SGR: Rose diagrams of surface orientation distribution of recrystallized grain boundaries (SURFOR analysis), and average aspect ratios of grains (PAROR analysis). Sections are perpendicular to foliation parallel and normal to lineation (*XZ* section, *YZ* section). Large scale shear sense on *XZ* sections (left column) is dextral. Local shear sense of sample 14.5 is sinistral (see text for explanation). Estimated temperatures of deformation and numbers of analyzed grains are indicated.

The orientations of the grain boundary surfaces were analyzed using the SURFOR method; the aspect ratios of the bulk fabric and of the individual grains as well as the orientations of the long axes of the grains, were analyzed using the PAROR program (Panozzo, 1983, 1984). SURFOR results are presented in the form of rose diagrams of surface orientation distribution function (surface ODF) and PAROR results as average grain aspect ratio (Fig. 11).

In sections perpendicular to the lineation (*Y–Z* sections; Fig. 11, right column), grains are flattened parallel (or subparallel) to the foliation. The average aspect ratio is approximately constant, varying slightly between 1.54 and 1.79. In sections parallel to the lineation (*X–Z* sections; Fig. 11, left column) flattening is more pronounced in an orientation oblique to the foliation. The aspect ratio increases steadily with increasing temperature of deformation, i.e. from 1.79 to 2.63, and the angle between the foliation and the flattening orientation decreases from 25° to 5°.

In *X–Z* sections, well developed preferred orientations of grain boundary surfaces and an oblique preferred orientation of grain long axes can be noted (rose diagrams, left column). The shear sense of sample 14-5 is reversed with

respect to the overall dextral shear sense in the strike slip zone. For sample 14-5, this reversal is in accordance with the texture and is explained as a local reversal of shear sense (see later discussion). The decreasing dispersion of surface ODFs in the $X–Z$ sections with increase in temperature of deformation (from sample 13-1 to 15-2) and the constant dispersion in the $Y–Z$ section is in agreement with the PAROR results, implying that grains are very well aligned, and increasingly elongated in the direction of the shear displacement with increasing shear strain.

None of the surface ODFs is symmetric about the first maximum preferred orientation. On the $X–Z$ section of sample 23-1, a secondary maximum at approximately 0–20° to the foliation normal is noticeable. The orientation with respect to the foliation normal is clockwise, corresponding to the dextral shear sense. In the other $X–Z$ sections (Fig. 11, left column), a secondary maximum is not recognizable as such; it only contributes to the asymmetry of the first maximum. With increasing temperature the asymmetry of the surface ODF decreases. On the $Y–Z$ sections (Fig. 11, right column), relatively strong secondary maxima are developed and none of the rose diagrams shows the 'hourglass constriction' that is typical of the surface ODF of the (strain) ellipse and indicative of intracrystalline plasticity (see discussion in Schmid et al., 1987).

The asymmetry, i.e. the occurrence of high angle secondary maxima in the surface ODFs, indicates that oblique subgrain boundaries are present (and visible) in the fabric (samples 23-1 and 14-5; Fig. 11). With increasing activity of grain boundary migration, the oblique submaximum decreases and the surface ODF becomes more symmetric (Stünitz, 1991). We suppose that these boundaries are formed by subgrain rotation during rhomb and basal ⟨a⟩ slip, two slip systems which are inferred to be active in the SGR zone (see later). With increasing temperature, prism ⟨a⟩ slip becomes active (e.g. Schmid and Casey, 1986). As the grain boundaries created by the latter system are invisible (Trépied et al., 1980), the secondary maximum of the surface ODF decreases and is another reason for the ODFs to become more symmetric (sample 15-2; Fig. 11).

Near the upper limit of the SGR zone, ribbon grains tend to be completely consumed by recrystallization and distinct fabric domains (cf. Pauli et al., 1996) start to develop. These fabric domains may represent former ribbon grains. Samples from the transition zone to GBM show far more variable grain shapes and sizes than in SGR (Fig. 7g). A broader range of recrystallized grain sizes was developed (85 μm $+60/-35$ μm). This is not typical for a clearly dominant subgrain rotation recrystallization process. It rather indicates a larger contribution of grain boundary migration, a process which tends to produce a wider distribution of recrystallized grain sizes. With increasing temperature the contribution of grain boundary migration increases and migration creates large-amplitude lobes.

At the transition from SGR to GBM the increase in grain size is discontinuous, just like the transition from BLG to SGR (Fig. 9). Such a discontinuity has also been found for olivine (Avé Lallement et al., 1980). Mercier (1980) and Hirth and Tullis (1992) suggest a stepped increase of the recrystallized grain size at transitions in the recrystallization mechanisms with increasing temperature. Comparable results for quartz have been described by Zulauf (2001).

4.4. Zone of grain boundary migration recrystallization (GBM)

Grain boundary migration recrystallization begins to dominate at around 500 to 550 °C. Within the GBM zone, the grain size distribution is broader than in the SGR zone. The grain boundaries are lobate and grain contacts are interfingering (Fig. 7g). Between 550 and 700 °C, the recrystallized grain size increases from a diameter of 220 μm up to a few millimeters (Fig. 9). The quartz veins are completely recrystallized above 550 °C (Fig. 10).

Increasing lobe size and interfingering lead to the formation of so-called 'island grains'. On a 2D section these grains appear as isolated grains ('dissection microstructure' described by Urai et al. (1986)). The recrystallized grain size increases more strongly with increasing temperature than in the SGR zone and reaches dimensions of a millimeter or even a few millimeters in diameter close to the pluton contact (Fig. 7h). Overgrowth and pinning of migrating grain boundaries by second phase particles are locally evident. The latter leads to locally smaller grain sizes (Fig. 7g; cf. White, 1979; Olgaard and Evans, 1988). Microstructures indicating the direction of migration, e.g. left-over grains (Urai, 1983), pinning-, window-, dragging- and castellate microstructures (Jessell, 1987), can be observed. No evidence for relict porphyroclasts can be found throughout the GBM zone. Intracrystalline deformation features, e.g. deformation lamellae and undulose and patchy extinction, are again attributed to a late deformational overprint under decreasing temperature conditions. Samples near or slightly above the transition from SGR to GBM also show subgrain boundaries. Some oblique fabrics resemble microstructures of SGR, but the angles between grain long axes and the main foliation in GBM fabrics are preferentially $>45°$. At higher temperatures no oblique fabrics are recognizable (Fig. 7h).

Even though grain boundaries are very lobate, they can exhibit straight segments which seem to be crystallographically controlled. At temperatures above 630 ± 30 °C, grain boundary pinning by obstacles like inclusions or grain boundaries is weak and migration and grain growth are practically unrestricted (Fig. 7h; see discussion section). Chessboard extinction is developed (Fig. 7i), which is a feature produced by high temperature subgrain formation; it has been explained by a combination of basal ⟨a⟩ and prism [c] slip (square subgrains of Blumenfeld et al. (1986) and Mainprice et al. (1986)). Kruhl (1996) relates chessboard extinction to the $\alpha–\beta$ transformation in quartz.

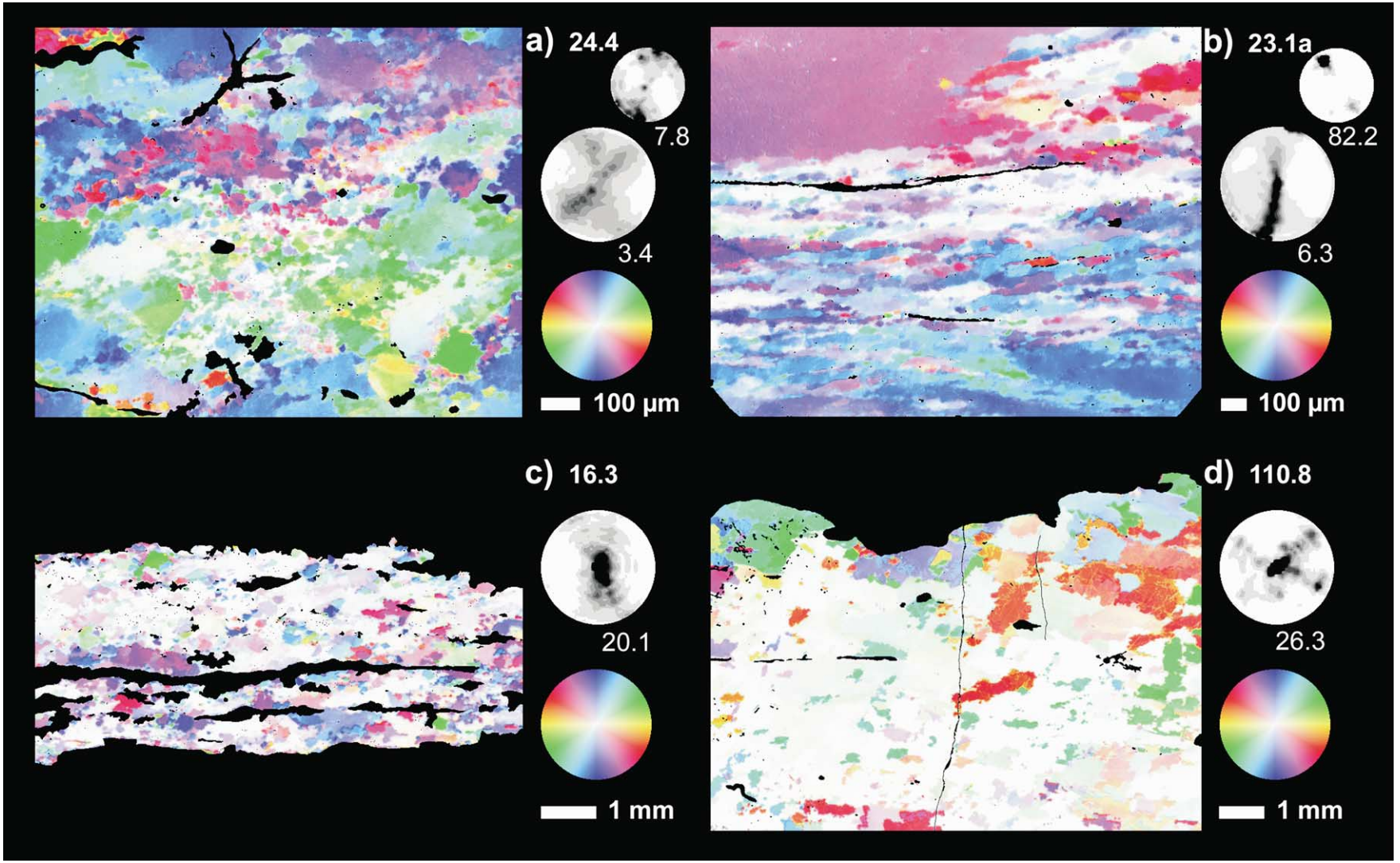

Fig. 12. CIP orientation images of quartz samples from different zones of dynamic recrystallization. Stereogram of color look-up table at lower right. [c]-axis pole figures are shaded in 0.5 intervals up to 4 × uniform, maxima are indicated below pole figures on the right. Sections are perpendicular to the foliation and parallel to the stretching lineation. Pole figures are in same orientation, lineation horizontal. The overall shear sense of the samples is dextral. Note the different scales. (a) Zone of high temperature BLG ($T \approx 400$ °C, sample 24.4). The small pole figure is a bulk [c]-axis pole figure from the represented orientation image, the large pole figure shows [c]-axes of the recrystallized grains. (b) Zone of SGR ($T \approx 460$ °C, sample 23.1). The small pole figure is a bulk [c]-axis pole figure from the represented orientation image. The large pole figure shows [c]-axes of the recrystallized grains. Ribbon grain (upper left corner, note the distinct maximum in the pole figure) and recrystallized grains (oblique single girdle in the pole figure) exhibit very different orientations. (c) Zone of GBM ($T \approx 560$ °C, sample 16.3), where quartz is completely recrystallized. Nearly white coloring corresponds to strong *Y* maximum of pole figure. (d) Zone of high temperature GBM ($T \approx 670$ °C, sample 110.8), within which quartz is completely recrystallized. Note appearance of peripheral maxima (red and green grains).

This influence is in accordance with the present study, because chessboard extinction only occurs in samples above the $\alpha-\beta$ transformation temperature ($T \approx 630$ °C at $P = 2.5$–3.0 kb).

5. Texture analysis

The crystallographic preferred orientation (CPO; referred to as texture in this paper) was investigated by a combination of computer integrated polarization (CIP) microscopy and X-ray texture goniometry. The fundamentals of the CIP method are explained in Panozzo Heilbronner and Pauli (1993, 1994). [c]-axis pole figures have been calculated from the CIP orientation images (Figs. 12 and 13a and b). Parts of the samples have been masked for a CIP analysis (Fig. 12) and separate [c]-axis pole figures were calculated for recrystallized grains and porphyroclasts. The X-ray texture analysis was carried out using a Siemens D5000 diffractometer. From the measured reflections {110}, {100}, {101} + {011} pole figures for a ⟨110⟩, m (100), c [001], r (101) and z (011) (Fig. 13a and b) were (re-)calculated using the software package MENTEX by Schaeben et al. (1990).

5.1. Texture of porphyroclasts

The X-ray pole figures of samples from the BLG and SGR zones (Fig. 13a) are dominated by the contribution of the porphyroclasts because recrystallized grains constitute less than 30% of the volume. Some of the specimens analyzed by texture goniometry (e.g. 14.5 of Fig. 13a) show a small number of strong maxima due to large porphyroclasts in the sample. In spite of the large grain size, statistically meaningful textures could be obtained by combining measurements from several sites within the same sample (e.g. sample 23.1a, b of Fig. 13a) and by comparing X-ray textures with CIP results (e.g. sample 24.4 of Fig. 13a).

The porphyroclasts within the BLG and SGR zones display maxima near the periphery in the [c]-axis pole figures and maxima subparallel to the foliation (*XY* plane) for the [m] and ⟨a⟩-axis pole figures (Fig. 13a). The [c]-axes can be found in a maximum subparallel to or at a small angle to *Z* (e.g. samples 26.2, 14.5 in Fig. 13a), or they form small circle orientations around *Z* (e.g. samples 27.1, 23.1b of Fig. 13a). The ⟨a⟩-axis pole figures for all the samples are similar, with maxima subparallel to the foliation, one of them typically lying near the lineation. These textures are interpreted to indicate dominant basal ⟨a⟩ slip, with some contribution from rhomb or π slip (cf. Schmid and Casey, 1986; Law et al., 1990). There is no dependence on temperature and no change with the transition from BLG to SGR (Fig. 13a). The small differences between the [c]- and between the ⟨a⟩-axis pole figures could reflect differences in the type of strain (*X*:*Y*:*Z* ratios, cf. Schmid and Casey, 1986). The main features of the porphyroclast-dominated texture type are shown in Fig. 14a.

5.2. Texture of recrystallized grains

In the low temperature part of the BLG zone the recrystallized grain size is too small to be analyzed by standard CIP methods. In order to separate textures of porphyroclasts from those of recrystallized domains in the high temperature BLG and in the SGR zone, CIP texture analysis was performed and separate pole figures were calculated for recrystallized grains and porphyroclasts (Fig. 12a and b). in combination with the X-ray data, an interpretation of the textural development of recrystallized grains and porphyroclasts is possible. The CIP-derived [c]-axis pole figures of recrystallized domains are compared with the [c]-axis pole figures obtained by X-ray goniometry in Fig. 13.

Sample 24.4 is the only sample in the BLG zone from which a CIP for recrystallized grains could be generated (Figs. 12a and 13a). The CIP-derived [c]-axis pole figure displays an asymmetric crossed girdle. The [c]-axis pole figures of recrystallized domains from the SGR zone exhibit asymmetric crossed girdles (samples 23.1, 14.5, 15.2 in Fig. 13) or single girdles (samples 13.1a or 23.1a in Figs. 12 and 13). The textures of recrystallized domains differ from those of the porphyroclasts in the BLG and SGR zones in that the [c]-axis positions of recrystallized grains are more dispersed along entire single or crossed girdles. The dispersion may be the result of the presence of fabric domains (Pauli et al., 1996). Alternatively, the girdle distribution of [c]-axes from recrystallized grains may indicate that more than one slip system (basal, rhomb and prism slip) operated. Two explanations of the texture differences between porphyroclasts and recrystallized grains are possible: (1) progressive subgrain rotation may have been effective in generating new orientations, or (2) porphyroclasts, with [c]-axis orientations unsuitable for slip on the basal plane preferentially recrystallized, thereby enriching porphyroclast orientations favorable for basal slip (Schmid, 1994; cf. Garcia Celma, 1982). Fig. 12b suggests that a combination of both interpretations, which are not mutually exclusive, is possible.

Near the transition from SGR to GBM (samples 15.2 and 21.2, Figs. 13b and 12c), the [c]-axis pole figure for recrystallized grains exhibits a transitional character between a single or crossed gridle distribution and a single maximum near *Y*. The still relatively diffuse *Y* maximum near the transition becomes increasingly narrow with increasing temperature within the GBM zone. Prism ⟨a⟩ slip most probably is the dominant slip system at these higher temperatures (e.g. Schmid and Casey, 1986).

Approaching 630 °C, where old grains are no more discernible, the *Y* maxima are very strong. Secondary maxima may appear at the periphery of the pole figures at small angles to the lineation (e.g. Fig. 12d; samples 18.5 and 66.3 in Fig. 13b). These maxima are indicative of prism [c] slip which is activated at high temperatures (cf. Schmid et al., 1981; Mainprice et al., 1986). The presence of the peripheral maxima also coincides with the chessboard

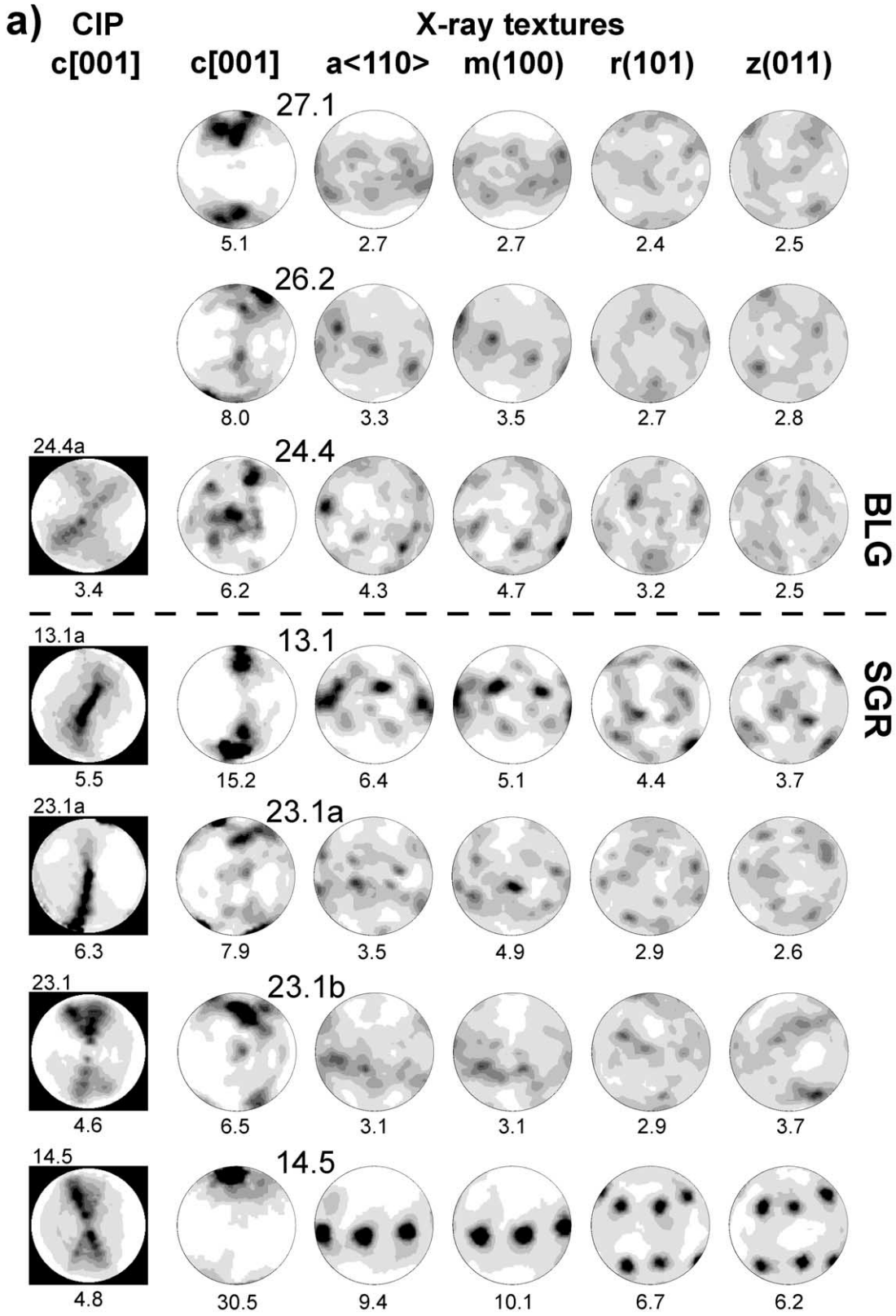

Fig. 13. CIP [c]-axis pole figures and X-ray goniometry measurements for specimens indicated in Fig. 3 (temperature increasing from top to bottom). Pole figures are shaded in 0.5 intervals up to 4 × uniform, magnitudes of maxima are given below pole figures. Sections are perpendicular to the foliation and parallel to the stretching lineation (*XZ* sections, with *X* horizontal); bulk shear sense of samples is dextral. CIP and X-ray goniometer measurements which are not derived from the same specimen are separated by vertical dashed lines. The letter 'a' in CIP sample numbers indicates pole figures of smaller sections representing more localized textures (fabric domains). CIP [c]-axis pole figures relate to recrystallized grains only. X-ray goniometry results are bulk textures. From sample 27.1 to sample 14.5 (a; BLG and SGR), pole figures reflect textures of porphyroclasts (volume proportion of the porphyroclasts is more than 50%), and from sample 58.1 to sample 21.4 (b; upper SGR and GBM), those of recrystallized grains (volume proportion of the recrystallized grains is more than 85%).

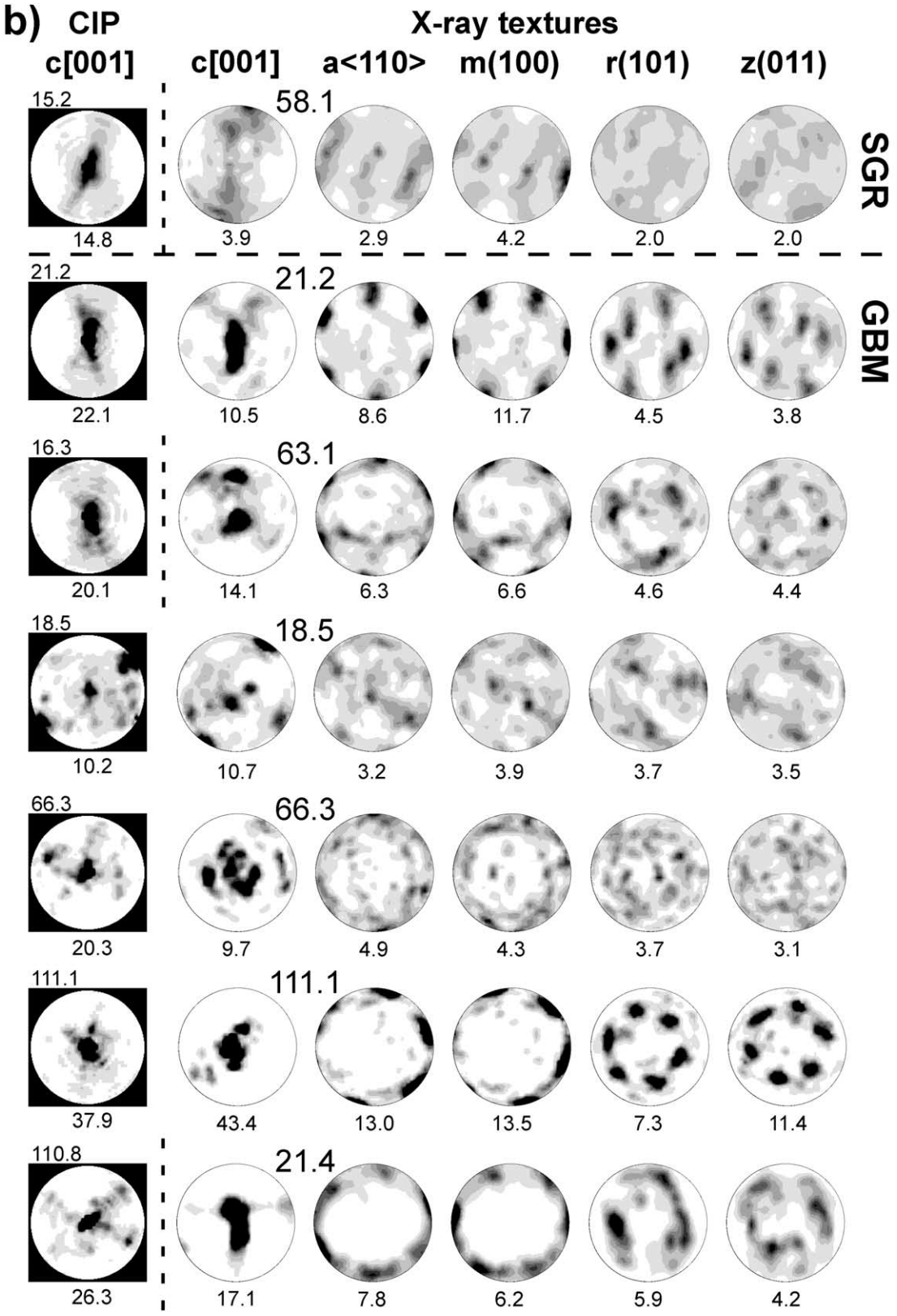

Fig. 13. (*continued*)

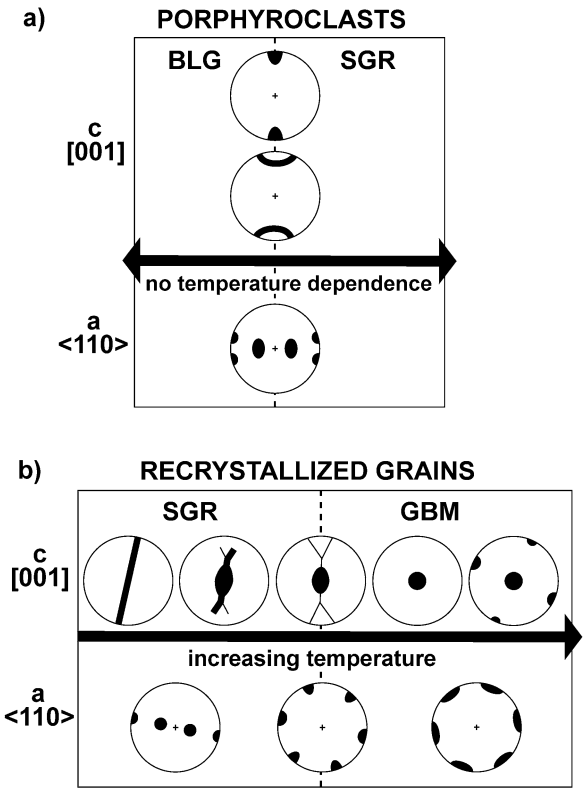

Fig. 14. (a) and (b) Schematic diagram of texture of the porphyroclasts and of the recrystallized grains with increasing temperature; for further explanation see text.

subgrains described earlier. The CIP pole figures show the development of these additional maxima more clearly than X-ray measurements, because the increase in grain size within the GBM zone renders X-ray goniometry difficult. The general trend from oblique single girdle [c]-axis pole figures to strong *Y* maxima, and finally into the more complex pole figures obtained at the highest temperatures, is schematically shown in Fig. 14b.

6. Discussion

6.1. Zone of cataclastic flow

The simultaneous occurrence of fracturing with localized crystal plastic deformation within the cataclastic fault zone corresponds to the 'semibrittle faulting' to 'semibrittle flow' behavior experimentally observed for quartz (e.g. Hirth and Tullis, 1994). Features such as undulose extinction and the beginning of dynamic recrystallization by grain boundary bulging indicate only that minor crystal plasticity contributes to total strain up to the temperature of 280 ± 30 °C, above which recovery features become dominant. The dominance of crystal plastic deformation is marked by the abrupt transition from cataclasites to mylonites on the mesoscopic scale. Thus, this study indicates that the transition from cataclasites to mylonites occurs over a narrow temperature range, implying that the transition in rheological properties (i.e. the frictional–viscous transition) is fairly sharp at constant depth.

Flow stresses derived by paleopiezometry from mylonites adjacent to the frictional–viscous transition reach values close to the pressures derived from the syn-deformational mineral assemblages (cf. Stipp, 2001; Stipp et al., 2002). Thus, the frictional–viscous transition observed in this study is compatible with the experimentally derived Goetze criterion which predicts this transition to occur when differential stress equals confining pressure (e.g. Kohlstedt et al., 1995). This agreement of experiments and natural deformation suggests that 'pressure' inferred from mineral assemblages in the mylonites corresponds to the effective confining pressure. Also, the microstructures indicative of the change from frictional wear to viscous creep correspond to those found in experimentally deformed quartz aggregates at the same transition (Hirth and Tullis, 1994). Fracturing within the SMZ close to the cataclastic Tonale fault may indicate that brittle deformation features accompany plastic deformation at the low temperature end of dislocation creep (McLaren and Pryer, 2001). These brittle features may have formed when differential stresses exceeded the effective confining pressure (cf. Küster and Stöckhert, 1999). Pseudotachylytes within the cataclastic Tonale fault (e.g. Müller, 1998) suggest that seismic events did occur.

6.2. Variations within the bulging recrystallization zone

Across the mylonitic fault zone and along the temperature gradient we mapped out three zones characterized by different recrystallization mechanisms. In the following sections we attempt to correlate these three recrystallization mechanisms and their associated microstructures and textures with the three experimentally defined dislocation creep regimes of Hirth and Tullis (1992) which have, among other criteria, been defined on the basis of different recrystallization mechanisms.

Small but significant microstructural differences exist between the lower and higher temperature parts of BLG. In the lower temperature part (BLG I), the proportion of recrystallized grains is very small and fracturing is still observed within individual porphyroclasts (Fig. 7b). The elongation of porphyroclasts by crystal plastic deformation is insignificant, hence most of the strain was probably taken up by the recrystallized fabric domains and to a lesser extent by frictional deformation. In the higher temperature part (BLG II), fracturing is unimportant or absent (Fig. 7c and d), and porphyroclasts show undulose and patchy extinction. Deformation lamellae are more common and porphyroclasts are considerably more elongated than in BLG I (Fig. 7c). Recrystallization is no longer localized at only a few sites along the grain boundaries (Fig. 7a and b); instead, the recrystallized grains surround the porphyroclasts, forming core and mantle structures (Fig. 7c and d). This is an

indication that subgrain rotation becomes more important with increasing temperature within BLG II, assuming constant strain rate conditions (cf. Hirth and Tullis, 1992; Stipp et al., 2002). Hirth and Tullis (1992) suggest that the transition from their regime 1 to regime 2 corresponds to a change from dominantly strain-induced grain boundary migration to dislocation-climb-accommodated recovery. We think that within the Tonale mylonites the same transition occurs between BLG I and BLG II within the BLG zone and that this transition is a gradual one. Hirth and Tullis (1992) also observed extensive crystal plastic deformation of porphyroclasts deforming in regime 2, whereas in regime 1 evidence of crystal plastic deformation of porphyroclasts is not prominent. This is exactly what we observe in the naturally deformed Tonale quartz specimens within the gradual transition from BLG I to BLG II.

6.3. The transition from bulging to subgrain rotation recrystallization

In contrast to the porphyroclasts in BLG II which are moderately elongated and display finely serrated grain boundaries, the porphyroclasts in the SGR zone may be extremely elongated ribbon grains (Fig. 7e). There, strain is primarily accommodated by basal ⟨a⟩ slip, while dynamic recrystallization was concentrated at triple junctions and along grain boundaries oriented at high angles to the foliation in the BLG zone (Fig. 7c and d). Recrystallization is no longer confined to grain boundaries at the onset of SGR. Instead, progressive subgrain rotation causes polygonization, commonly resulting in complete recrystallization of the porphyroclasts (Fig. 7e and f). As polygonization affects entire grains, the volume proportion of recrystallized grains within the SGR zone increases more strongly than within BLG (Figs. 7e and f and 10). The SGR zone is correlated with regime 2 of Hirth and Tullis (1992). Thus, in naturally deformed rocks, regime 2 encompasses the upper part of the BLG zone (BLG II) and the SGR zone.

Across the BLG/SGR-transition of the Tonale mylonites we found a discontinuity with regard to the slope of the recrystallized grain size temperature relationship (Fig. 9). This change in slope is taken as one criterion to distinguish between BLG and SGR recrystallization mechansims in this study.

6.4. The transition from subgrain rotation to grain boundary migration recrystallization

In the Tonale mylonites, the SGR/GBM-transition is well defined microstructurally. Samples near this transition, characterized by recrystallized grains of uniform size and shape and some small-scale sutures at the grain boundaries, can be correlated with the regime 3 microstructures of Hirth and Tullis (1992). Since these authors proposed the combined occurrence of subgrain rotation and grain boundary migration recrystallization for their regime 3 we conclude that their regime 3 corresponds to our transition from SGR to GBM. Close to the SGR/GBM-transition within GBM, substantially more subgrains can be found compared with the higher temperature part of GBM (Fig. 7h). This may be related to higher grain boundary migration velocities at higher temperature, causing migration to outweigh subgrain formation. To the best of our knowledge, typical high temperature GBM microstructures, such as those found along the Tonale fault zone, including dissection microstructures (Urai et al., 1986), left-over grains, dragging microstructures (Jessell, 1987), have not been produced in quartz deformation experiments. Laboratory strain rates at similarly low stresses would require very high deformation temperatures where partial melting would preclude the formation of high temperature grain boundary migration recrystallization microstructures.

The SGR/GBM-transition is also characterized by a change in slope of the recrystallized grain size temperature relationship (Fig. 9). Furthermore, the texture of the recrystallized grains displays a rather abrupt change from single or crossed girdle [c]-axes to the formation of a [c]-axis *Y* maximum indicative of prism ⟨a⟩ slip (Schmid et al., 1981; Figs. 12 and 14a and b). The simultaneous changes in dynamic recrystallization and texture imply an effect of the specific recrystallization mechanism on texture formation or, conversely, an effect of the operating slip systems on the recrystallization mechanism (see later discussion).

6.5. Variations within the zone of grain boundary migration recrystallization

The GBM zone displays slight microstructural changes from the lower to the higher temperature part (here termed GBM I and GBM II, respectively). At lower temperatures, grain sizes and shapes are variable, but outlines of single grains are still detectable. At higher temperatures, grains acquire large sizes and irregular amoeboid shapes. Hence, it becomes difficult to define individual grains. Dissection microstructures with island grains are typical. Due to boundaries breaking away from second phase particles, substantial grain growth may occur. As pinning is important in GBM I and nearly absent in GBM II, the transition of impurity-controlled to not-impurity-controlled grain boundary migration (Lücke and Stüwe, 1971; Poirier and Guillopé, 1979) is inferred to occur within the GBM zone in naturally deformed rocks, and not at the SGR/GBM-transition as proposed by Hirth and Tullis (1992) for their experimental transition from regime 2 to regime 3. Not-impurity-controlled grain boundary migration can be induced by an increase in temperature or a change in misorientation or by an increase in the internal strain energy as pointed out by Urai et al. (1986). An increase in temperature from GBM I to GBM II is obvious from the metamorphic data. A higher frequency of misorientation changes and an

increase in internal strain energy will be discussed in Section 6.6.

From lower to higher temperatures within the GBM zone the texture displays a change from [c]-axis pole figures with a strong single *Y* maximum indicative of prism ⟨a⟩ slip towards pole figures with additional secondary maxima. The latter are indicative of combined basal ⟨a⟩ and prism [c] slip. We propose that this changeover is related to the α–β transformation in quartz (Kruhl, 1996) rather than to a change in recrystallization mechanism.

6.6. Implications regarding the interpretation of textures

Our texture analysis confirms a dominant dextral sense of shear, corresponding to the shear sense which has been established all along the eastern tonale fault zone (e.g. Schmid et al., 1989; Werling, 1992). A dextral sense of shear can be also derived from other independent shear sense indicators such as rotated porphyroclasts and shear bands. However, a few samples show the opposite shear sense, possibly caused by local inhomogeneities such as folding or porphyroclast-related effects (e.g. Garcia Celma, 1982; Hippertt and Tohver, 1999) or domainal fabrics (e.g. Pauli et al., 1996).

The texture of the porphyroclasts does not indicate significant changes in the active slip systems with increasing temperature up to the transition into the GBM zone at around 500 °C. This suggests that slip along the basal plane is probably responsible for the deformation of elongated ribbon grains. On the other hand, the texture of the recrystallized grains displays a sequence of activated slip systems with increasing temperature which is discussed by Hobbs (1985) and Schmid (1994) on the basis of single crystal experiments (e.g. Baëta and Ashby, 1969; Hobbs et al., 1972; Blacic, 1975) and on the basis of the texture analysis on natural polycrystals (e.g. Schmid and Casey, 1986), respectively. The sequence of slip systems in non-coaxial plane strain deformation with increasing temperature can be summarized as follows: basal (c) ⟨a⟩ slip in porphyroclasts (not in recrystallized grains which deform by combined basal, rhomb and prism ⟨a⟩ slip), prism {m} ⟨a⟩ slip, and at high temperatures (in our study above 630 ± 30 °C) prism {m} ⟨c⟩ slip. The transition to single maxima in *Y* in the [c]-axis pole figures is abrupt. It suggests a change from combined basal, rhomb and prism ⟨a⟩ slip to dominant prism ⟨a⟩ slip for the recrystallized grains and coincides with the transition to the GBM zone at around 500 °C.

The texture becomes stronger with increasing temperature (cf. Jessell, 1987) and there is no evidence of texture weakening by an increasing mobility of grain boundaries, as found experimentally by Gleason et al. (1993). The coinciding transitions of dynamic recrystallization microstructures and texture types with increasing temperatures suggest that there is an interaction between dynamic recrystallization and dislocation-creep-induced texture formation (Schmid and Casey, 1986; Urai et al., 1986; Schmid, 1994). It is interesting to note that the most important change in slip systems occurs with the transition in the dominant recrystallization mechanism from SGR to GBM. The activity of more than one independent slip system in the recrystallized grains of the SGR zone may be necessary for strain compatibility. Diffusional mass transfer is probably not fast enough within the SGR zone to ensure this compatibility, but it may contribute to it locally (cf. Means and Jessell, 1986). At higher temperatures and within the GBM zone, strain compatibility between different grains can be accommodated by relatively fast migration, i.e. by the removal of grains. The change from multiple active slip systems to a single slip system may also be due to the selective removal of certain orientations by grain boundary migration recrystallization (Knipe and Law, 1987; Schmid et al., 1987). Grains that deform by multiple slip systems probably build up higher internal strain energy than grains with only one dominant slip system (Kamb, 1972; Nicolas and Poirier, 1976). Assuming that grain boundary migration is driven by the reduction in stored strain energy, strained grains with multiple slip systems may be consumed by grains with single active slip systems (cf. Urai et al., 1986). This process could strengthen the single *Y* maximum. In any case, the coincidence of the switch to the single *Y* maximum with the transition in recrystallization towards GBM suggests a strong coupling between the dominant recrystallization mechanism and texture formation.

The change from GBM I to GBM II coincides with a switch from single towards multiple slip (i.e. from prism ⟨a⟩ slip to a combination of prism ⟨a⟩ slip, prism [c] and basal ⟨a⟩ slip). Hence, grains are expected to store higher internal strain energy in GBM II where the texture does not indicate that grains with multiple systems are consumed by grains deformed by a single slip system. Instead, the increase in internal strain energy may contribute to a higher mobility of grain boundaries. Thus, the increase in the mobility of migrating grain boundaries in GBM II could be caused by the activation of combined prism [c] and basal ⟨a⟩ slip, in addition to prism ⟨a⟩ slip, but also by the temperature increase. This higher grain boundary mobility may allow the changeover from impurity to not-impurity-controlled grain boundary migration recrystallization.

6.7. Remarks on correlation between nature and experiment

The observed recrystallization microstructures can be correlated with the experimental dislocation creep regimes of Hirth and Tullis (1992). Similar microstructural variations in other tectonometamorphic settings have also been described and correlated to the experimental dislocation creep regimes (e.g. Dunlap et al., 1997; Stöckhert et al., 1999; Zulauf, 2001). It appears that dynamic recrystallization microstructures of quartz are a relatively robust feature in natural fault zones despite later modifications such as retrograde overprinting or annealing, as pointed out by Stöckhert et al. (1999).

The temperature intervals where certain microfabrics are produced do not coincide between nature and experiment because of the compensation of temperature for strain rate. Under the high strain rate conditions which are required for experiments relatively higher temperatures are necessary to activate deformation mechanisms similar to those found in nature. Using paleopiezometers and experimentally calibrated flow laws a stress and strain rate estimation can be carried out for mylonitic fault zones (e.g. Hacker et al. 1990, 1992; Prior et al., 1990; Dunlap et al., 1997; Stöckhert et al., 1999; Zulauf, 2001). Stresses and strain rates have also been determined for the Tonale mylonites and by the link of the dynamic recrystallization microstructures the deformation conditions in nature can be extrapolated to those of experimental rock deformation (cf. Hirth et al., 2001; Stipp, 2001; Stipp et al., 2002). In many other mylonite belts, however, deformation conditions are not so well constrained. In spite of possible variations in stress and strain rate during natural rock deformation we are convinced that the Tonale fault zone is representative of most mylonite belts. It is reasonable to assume that stress and strain rate conditions in the Tonale fault zone are within the common natural range widely observed for natural shear zones (flow stresses up to 200 MPa and strain rates between 10^{-14} and 10^{-11} s^{-1}, e.g. Mercier et al., 1977; Pfiffner and Ramsay, 1982; Hacker et al., 1990, 1992; Prior et al., 1990; Dunlap et al., 1997; Küster and Stöckhert, 1999; Stöckhert et al., 1999; Zulauf, 2001; Stipp et al., 2002). Hence, we propose that the temperature range given in this work may be used in order to derive, at least in an approximate way, the deformation temperatures in mylonites for which no other temperature constraints, such as syntectonic mineral parageneses are available.

7. Summary and conclusions

The natural laboratory provided by the Tonale fault zone was active during the intrusion of the adjacent Adamello pluton. It provides an opportunity to study natural quartz deformation microstructures and textures over a temperature range from approximately 250 °C to about 700 °C across the Eastern Tonale fault zone. The frictional–viscous transition, i.e. the transition from cataclasites to mylonites, occurs at ~280 °C.

In the fault zone, the changes in the dominant type of dynamic recrystallization correspond to progressively increasing temperatures derived from mineral parageneses formed during syn-kinematic contact metamorphism. The fault zone is subdivided into three zones on the basis of microstructures that record different dynamic recrystallization mechanisms: dominant bulging recrystallization (BLG) from ~280 to ~400 °C, dominant subgrain rotation recrystallization (SGR) from ~400 to ~500 °C, and dominant grain boundary migration recrystallization (GBM) from ~500 to ~700 °C. The BLG/SGR-transition as well as the SGR/GBM-transition are marked by a change in slope in the temperature dependence of the recrystallized grain size.

Dynamic recrystallization microstructures are correlated with the experimental dislocation creep regimes of Hirth and Tullis (1992). The zone of BLG is characterized by local grain boundary bulging leading to small-scale serrations. An increasing contribution of subgrain rotation in the BLG zone is used to separate a lower (BLG I) from a higher temperature part (BLG II). BLG I and BLG II are correlated to regime 1 and the lower temperature part of regime 2, respectively, of the experimental dislocation creep regimes. SGR is characterized by the polygonization of ribbon grains, recrystallized grains and subgrains are of equal size and shape. The zone of SGR is correlated to the higher temperature part of regime 2 of the experimental dislocation creep regimes. Regime 3 microstructures correspond to samples from the SGR/GBM-transition. However, most microstructures of the GBM zone found in this study have not been produced experimentally. Microstructures characteristic for the GBM zone are large-scale grain boundary sutures, irregular grain shapes, island grains and dissection microstructures. Variations in the natural GBM microstructures with the deformation temperature facilitate the distinction between a lower and higher temperature subzone. This change occurs near the $\alpha-\beta$ transformation of quartz and is documented by chessboard microstructures which form from subgrains during the activity of combined prism [c] and basal ⟨a⟩ slip.

Porphyroclasts and ribbon grains exhibit a texture consistent with basal slip, independent of temperature up to approximately 550 °C above which rocks are completely recrystallized. In contrast, the texture of the recrystallized grains depends on the deformation temperature and on the dominant recrystallization mechanism. The change from [c]-axis girdle pole figures to single maxima in *Y* in the recrystallized domains can be interpreted as a change from multiple slip systems (combined basal, rhomb and prism ⟨a⟩ slip) to a single active slip system (prism ⟨a⟩ slip), coinciding with the SGR/GBM transition at about 500 °C.

Acknowledgements

We are grateful to Elmar Werling who first discovered the syn-kinematic shearing and contact metamorphism at the eastern Tonale Line and whose pioneering work initiated the present analysis. Many fruitful discussions with Jan Tullis and Greg Hirth helped to clarify correlations between natural and experimental microstructures. Thorough and constructive reviews by Laurel Goodwin and Bernhard Stöckhert significantly improved the paper. For technical support we thank Hans Rudi Rüegg and Willy Tschudin. Thorsten Nagel is thanked for assistance and advice at the

microprobe and Jeanette Schaub for digitizing grain boundary outlines. This work was funded by the Swiss National Science Foundation, grant nos. 20-49562.96 and 2000-055420.98.

References

Avé Lallement, H.G., Mercier, J.-C.C., Carter, N.L., Ross, J.V., 1980. Rheology of the upper mantle: inference from peridotite xenoliths. Tectonophysics 70, 85–113.

Baëta, R.D., Ashby, K.H.G., 1969. Slip systems in quartz: I. experiments. American Mineralogist 54, 1551–1573.

Bailey, J.E., Hirsch, P.B., 1962. The recrystallization process in some polycrystalline metals. Proceedings of the Royal Society of London A 267, 11–30.

Blacic, J.D., 1975. Plastic-deformation mechanisms in quartz: the effect of water. Tectonophysics 27, 271–294.

Blumenfeld, P., Mainprice, D., Bouchez, J.L., 1986. C-slip in quartz from subsolidus deformed granite. Tectonophysics 127, 97–115.

Bohlen, S.R., Montana, A., Kerrick, D.M., 1991. Precise determinations of the equilibria kyanite–sillimanite and kyanite–andalusite and a revised triple point for Al_2SiO_5 polymorphs. American Mineralogist 76, 677–680.

Bucher, K., Frey, M., 1994. Petrogenesis of Metamorphic Rocks. Springer-Verlag, Berlin, Heidelberg, New York 318pp.

Cahn, R.W., 1983. Recovery and recrystallization. In: Cahn, R.W. Haasen, P. (Eds.), Physical Metallurgy. Elsevier Science Publishers BV., pp. 1596–1671

Carter, N.L., Kirby, S.H., 1978. Transient creep and semibrittle behavior of crystalline rocks. Pure and Applied Geophysics 116, 807–839.

Chatterjee, N.D., Johannes, W., 1974. Thermal stability and standard thermodynamic properties of synthetic $2M_1$-muscovite, $KAl_2[AlSi_3O_{10}(OH)_2]$. Contributions to Mineralogy and Petrology 48, 89–114.

Drury, M.R., Humphreys, F.J., 1986. The development of microstructure in Al–5% Mg during high temperature deformation. Acta Metallurgica 34, 2259–2271.

Drury, M.R., Urai, J.L., 1990. Deformation-related recrystallization processes. Tectonophysics 172, 235–253.

Drury, M.R., Humphreys, F.J., White, S.H., 1985. Large strain deformation studies using polycrystalline magnesium as a rock analogue. Part II: dynamic recrystallisation mechanisms at high temperatures. Physics of the Earth and Planetary Interiors 40, 208–222.

Dunlap, W.J., Hirth, G., Teyssier, C., 1997. Thermomechanical evolution of a ductile duplex. Tectonics 16, 983–1000.

Etheridge, M.A., Wilkie, J.C., 1981. An assessment of dynamically recrystallized grainsize as a paleopiezometer in quartz-bearing mylonite zones. Tectonophysics 78, 475–508.

Fitz Gerald, J.D., Stünitz, H., 1993. Deformation of granitoids at low metamorphic grade. I: reactions and grain size reduction. Tectonophysics 221, 269–297.

Garcia Celma, A., 1982. Domainal and fabric heterogeneities in the Cap de Creus quartz mylonites. Journal of Structural Geology 44, 443–456.

Gifkins, R.C., 1976. Grain boundary sliding and its accommodation during creep and superplasticity. Metallurgical Transactions 7A, 1225–1232.

Gleason, G.C., Tullis, J.H., Heidelbach, F., 1993. The role of dynamic recrystallization in the development of lattice preferred orientations in experimentally deformed quartz aggregates. Journal of Structural Geology 15, 1145–1168.

Guillopé, M., Poirier, J.P., 1979. Dynamic recrystallization during creep of single-crystalline halite: an experimental study. Journal of Geophysical Research 84, 5557–5567.

Hacker, B.R., Yin, A., Christie, J.M., Snoke, A.W., 1990. Differential stress, strain rate, and temperatures of mylonitization in the Ruby Mountains, Nevada: implications for the rate and duration of uplift. Journal of Geophysical Research 95, 8569–8580.

Hacker, B.R., Yin, A., Christie, J.M., Davis, G.A., 1992. Stress magnitude, strain rate, and rheology of extended middle continental crust inferred from quartz grain sizes in the Whipple Mountains, California. Tectonics 11, 36–46.

Heitzmann, P., 1987. Evidence of late Oligocene/early Miocene backthrusting in the central Alpine "root zone". Geodynamica Acta 1, 183–192.

Hippertt, J., Tohver, E., 1999. On the development of zones of reverse shearing in mylonitic rocks. Journal of Structural Geology 21, 1603–1614.

Hirth, G., Tullis, J., 1992. Dislocation creep regimes in quartz aggregates. Journal of Structural Geology 14, 145–159.

Hirth, G., Tullis, J., 1994. The brittle–plastic transition in experimentally deformed quartz aggregates. Journal of Geophysical Research 99, 11731–11747.

Hirth, G., Teyssier, C., Dunlap, W.J., 2001. An evaluation of quartzite flow laws based on comparisons between experimentally and naturally deformed rocks. International Journal of Earth Sciences 90, 77–87.

Hobbs, B.E., 1968. Recrystallization of single crystal of quartz. Tectonophysics 6, 353–401.

Hobbs, B.E., 1985. The geological significance of microfabric analysis. In: Wenk, H.-R. (Ed.). Preferred Orientation in Deformed Metals and Rocks: An Introduction to Modern Texture Analysis. Academic Press, Orlando, pp. 463–484.

Hobbs, B.E., McLaren, A.C., Paterson, M.S., 1972. Plasticity of single crystals of synthetic quartz. In: Heard, H.C., Borg, I.Y., Carter, N.L., Raleigh C.B. (Eds.), Flow and Fracture of Rocks. Geophysical Monograph 16, pp. 29–53.

Holland, T.J.B., Powell, R., 1990. An enlarged and updated internally consistent thermodynamic dataset with uncertainties and correlations: the system K_2O- Na_2O- CaO- MgO- MnO- FeO- Fe_2O_3- Al_2O_3- TiO_2- SiO_2- C- H_2- O_2. Jounal of Metamorphic Geology 8, 89–124.

Jessell, M.W., 1987. Grain-boundary migration microstructures in a naturally deformed quartzite. Journal of Structural Geology 9, 1007–1014.

Johannes, W., 1989. Melting of plagioclase–quartz assemblages at 2 kbar water pressure. Contributions to Mineralogy and Petrology 103, 270–276.

Johannes, W., Holtz, F., 1996. Petrogenesis and Experimental Petrology of Granitic Rocks. Minerals and Rocks. Springer-Verlag, Berlin, Heidelberg, New York 335pp.

Kamb, B., 1972. Experimental recrystallization of ice under stress. In: Heard, H.C., Borg, I.Y., Carter, N.L., Raleigh C.B. (Eds.), Flow and Fracture of Rocks. Geophysical Monograph 16, pp. 211–241.

Kerrick, D.M., 1990. The Al_2SiO_5 polymorphs. Reviews in Mineralogy 22. Mineralogical Society of America, 406pp.

Kerrick, D.M., Heninger, S.G., 1984. The andalusite–sillimanite equilibrium revisited. Geological Society of America Abstracts 16, 558.

Knipe, R.J., Law, R.D., 1987. The influence of crystallographic orientation and grain boundary migration on microstructural and textural evolution in an *S–C* mylonite. Tectonophysics 135, 155–169.

Kohlstedt, D.L., Evans, B., Mackwell, S.J., 1995. Strength of the lithosphere: constraints imposed by laboratory experiments. Journal of Geophysical Research 100, 17587–17602.

Kretz, R., 1983. Symbols for rock forming minerals. American Mineralogist 68, 277–279.

Kruhl, J.H., 1996. Prism- and basal-plane parallel subgrain boundaries in quartz: a microstructural geothermobarometer. Journal of Metamorphic Geology 14, 581–589.

Küster, M., Stöckhert, B., 1999. High differential stress and sublithostatic pore fluid pressure in the ductile regime—microstructural evidence for short-term post-seismic creep in the Sesia Zone, Western Alps. Tectonophysics 303, 263–277.

Law, R.D., Schmid, S.M., Wheeler, J., 1990. Simple shear deformation and quartz crystallographic fabrics: a possible natural example from the Torridon area of NW Scotland. Journal of Structural Geology 12, 29–45.

Lücke, K., Stüwe, H.P., 1971. On the theory of impurity controlled grain boundary motion. Acta Metallurgica 19, 1087–1099.

Mainprice, D.H., Bouchez, J.-L., Blumenfeld, P., Tubiá, J.M., 1986. Dominant c slip in naturally deformed quartz: implications for dramatic plastic softening at high temperature. Geology 14, 819–822.

Martin, S., Prosser, G., Santini, L., 1991. Alpine deformation along the Periadriatic lineament in the Italian Eastern Alps. Annales Tectonicae 5, 118–140.

McLaren, A.C., Pryer, L.L., 2001. Microstructural investigation of the interaction and interdependence of cataclastic and plastic mechanisms in Feldspar crystals deformed in the semi-brittle field. Tectonophysics 335, 1–15.

Means, W.D., 1981. The concept of steady-state foliation. Tectonophysics 78, 179–200.

Means, W.D., 1983. Microstructure and micromotion in recrystallization flow of Octachloropropane: a first look. Geologische Rundschau 72, 511–528.

Means, W.D., Jessell, M.W., 1986. Accommodation migration of grain boundaries. Tectonophysics 127, 67–86.

Mendum, J.R., 1976. The Structure and Metamorphic Geology of the Tonale Pass Area, Northern Italy. Ph.D. Thesis, University of Edinburgh.

Mercier, J.-C.C., 1980. Magnitude of continental lithospheric stress inferred from rheomorphic petrology. Journal of Geophysical Research 85, 6293–6303.

Mercier, J.-C.C., Anderson, D.A., Carter, N.L., 1977. Stress in the lithosphere: inferences from steady state flow of rocks. Pure and Applied Geophysics 115, 199–226.

Merriman, R.J., Frey, M., 1999. Patterns of very low-grade metamorphism in metapelitic rocks. In: Frey, M., Robinson, D. (Eds.). Low-Grade Metamorphism. Blackwell Science Ltd, pp. 61–107.

Müller, W., 1998. Isotopic Dating of Deformation Using Microsampling Techniques: The Evolution of the Periadriatic Fault System (Alps). Ph.D. thesis, ETH Zürich.

Nicolas, A., Poirier, J.P., 1976. Crystalline Plasticity and Solid State Flow in Metamorphic Rocks. John Wiley & Sons, London 444pp.

Nishikawa, O., Takeshita, T., 2000. Progressive lattice misorientation and microstructural development in quartz veins deformed under subgreenschist conditions. Journal of Structural Geology 22, 259–276.

Olgaard, D.L., Evans, B., 1988. Grain growth in synthetic marbles with added mica and water. Contributions to Mineralogy and Petrology 100, 246–260.

Ord, A., Christie, J.M., 1984. Flow stresses from microstructures in mylonitic quartzites of the Moine Thrust zone, Assynt area, Scotland. Journal of Structural Geology 6, 639–654.

Panozzo, R., 1983. Two-dimensional analysis of shape-fabric using projections of digitized lines in a plane. Tectonophysics 95, 279–294.

Panozzo, R., 1984. Two-dimensional strain from the orientation of lines in a plane. Journal of Structural Geology 6, 215–221.

Panozzo Heilbronner, R., Pauli, C., 1993. Integrated spatial and orientation analysis of quartz [c]-axes by computer-aided microscopy. Journal of Structural Geology 15, 369–382.

Panozzo Heilbronner, R., Pauli, C., 1994. Orientation and misorientation imaging: integration of microstructural and textural analysis. In: Bunge, H.J., Siegesmund, S., Skrotzki, W., Weber, K. (Eds.). Textures of Geological Materials. DGM Informationsgesellschaft Verlag, Oberursel, pp. 147–164.

Patiño Douce, A.E., Harris, N., 1998. Experimental constraints on Himalayan anatexis. Journal of Petrology 39, 689–710.

Pattison, D.R.M., Tracy, R.J., 1991. Phase equilibria and thermobarometry of metapelites. In: Kerrick, D.M. (Ed.), Contact Metamorphism. Reviews in Mineralogy 26. Mineralogical Society of America, pp. 105–206.

Pauli, C., Schmid, S.M., Panozzo Heilbronner, R., 1996. Fabric domains in quartz mylonites: localized three dimensional analysis of microstructure and texture. Journal of Structural Geology 18, 1183–1203.

Pfiffner, O.A., Ramsay, J.G., 1982. Constraints on geological strain rates: arguments from finite-strain states of naturally deformed rocks. Journal of Geophysical Research 87, 311–321.

Poirier, J.P., 1985. Creep of Crystals. Cambridge University Press, Cambridge 260pp.

Poirier, J.P., Guillopé, M., 1979. Deformation-induced recrystallization of minerals. Bulletin de Minéralogie 102, 67–74.

Poirier, J.P., Nicolas, A., 1975. Deformation-induced recrystallization by progressive misorientation of subgrain-boundaries, with special reference to mantle peridotites. Journal of Geology 83, 707–720.

Prior, D.J., Knipe, R.J., Handy, M.R., 1990. Estimates of the rates of microstructural changes in mylonites. In: Knipe, R.J., Rutter E.H. (Eds.), Deformation Mechanisms, Rheology and Tectonics. Special Publications of the Geological Society of London 54, pp. 309–319.

Rasband, W., 1996. NIH Image. National Institute of Health, Research Services Branch NIMH.

Schaeben, H., Siemes, H., Höfler, S., Will, G., 1990. Practical application of entropy optimization in quantitative texture analysis. In: Knipe, R.J., Rutter E.H. (Eds.), Deformation Mechanisms, Rheology and Tectonics. Special Publications of the Geological Society of London 54, pp. 375–381.

Schmid, S.M., 1994. Textures of geological materials: computer model predictions versus empirical interpretations based on rock deformation experiments and field studies. In: Bunge, H.J., Siegesmund, S., Skrotzki, W., Weber, K. (Eds.). Textures of Geological Materials. DGM Informationsgesellschaft Verlag, Oberursel, pp. 279–301.

Schmid, S.M., Casey, M., 1986. Complete fabric analysis of some commonly observed quartz [c]-axis patterns. In: Hobbs, B.E., Heard H.C. (Eds.), Mineral and Rock Deformation: Laboratory Studies. Geophysical Monograph 36, pp. 263–286.

Schmid, S.M., Handy, M.R., 1991. Towards a genetic classification of fault rocks: geological usage and tectonophysical implications. In: Müller, D.W., McKenzie, J.A., Weissert, H. (Eds.). Controversies in Modern Geology. Academic Press, London, pp. 339–361.

Schmid, S.M., Paterson, M.S., Boland, J.N., 1980. High temperature flow and dynamic recrystallization in Carrara marble. Tectonophysics 65, 245–280.

Schmid, S.M., Casey, M., Starkey, J., 1981. An illustration of the advantages of a complete texture analysis described by the orientation distribution function (ODF) using quartz pole figure data. Tectonophysics 78, 101–117.

Schmid, S.M., Panozzo, R., Bauer, S., 1987. Simple shear experiments on calcite rocks: rheology and microfabric. Journal of Structural Geology 9, 747–778.

Schmid, S.M., Aebli, H.R., Heller, F., Zingg, A., 1989. The role of the Periadriatic Line in the tectonic evolution of the Alps. In: Coward, M.P., Dietrich, D., Park R.G. (Eds.), Alpine Tectonics. Special Publications of the Geological Society of London 45, pp. 153–171.

Spear, F.S., Cheney, J.T., 1989. A petrogenetic grid for pelitic schists in the system SiO_2–Al_2O_3–FeO–MgO–K_2O–H_2O. Contributions to Mineralogy and Petrology 101, 149–164.

Stipp, M., 2001. Dynamic recrystallization of quartz in fault rocks from the Eastern Tonale Line (Italian Alps) Ph.D. thesis, University of Basel.

Stipp, M., Schmid, S., 1998. Evidence for the contemporaneity of movements along the Tonale line and the intrusion of parts of the Adamello batholith. Memorie di Scienze Geologiche 50, 89–90.

Stipp, M., Stünitz, H., Heilbronner, R., Schmid, S.M., 2002. Dynamic recrystallization of quartz: correlation between natural and experimental conditions. In: De Meer, S., Drury, M.R., De Bresser, J.H.P., Pennock, G.M. (Eds.) Deformation Mechanisms, Rheology and Tectonics: Current Status and Future Perspectives. Special Publications of the Geological Society of London.

Stöckhert, B., Brix, M.R., Kleinschrodt, R., Hurford, A.J., Wirth, R., 1999. Thermochronometry and microstructures of quartz—a comparison with experimental flow laws and predictions on the temperature of the brittle–plastic transition. Journal of Structural Geology 21, 351–369.

Stünitz, H., 1991. Folding and shear deformation in quartzites, inferred from crystallographic preferred orientation and shape fabric. Journal of Structural Geology 13, 71–86.

Thompson, J.B., Norton, S.A., 1968. Paleozoic regional metamorphism in

New England and adjacent areas. In: Zen, E.-a., White, W.S., Hadley, J.B., Thompson, J.B.J. (Eds.), Studies of Appalachian Geology: Northern and Maritime. Interscience Publishers, pp 319–327.

Trener, G.B., 1906. Geologische Aufnahme im nördlichen Abhang der Presanellagruppe. Jahrbuch der Kaiserlich-Königlichen Geologischen Reichsanstalt 56, 405–496.

Trépied, L., Doukhan, J.C., Paquet, J., 1980. Subgrain boundaries in quartz—theoretical analysis and microscopic observations. Physics and Chemistry of Minerals 5, 201–218.

Tullis, J., Yund, R.A., 1985. Dynamic recrystallization of feldspar—a mechanism for ductile shear zone formation. Geology 13, 238–241.

Tungatt, P.D., Humphreys, F.J., 1984. The plastic deformation and dynamic recrystallisation of polycrystalline sodium nitrate. Acta Metallurgica 32, 1625–1635.

Urai, J.L., 1983. Deformation of Wet Salt Rocks. Ph.D. Thesis, University of Utrecht.

Urai, J.L., Means, W.D., Lister, G.S., 1986. Dynamic recrystallization of minerals. In: Hobbs, B.E., Heard H.C. (Eds.), Mineral and Rock Deformation: Laboratory Studies. Geophysical Monograph 36, pp. 161–199.

van Daalen, M., Heilbronner, R., Kunze, K., 1999. Orientation analysis of localized shear deformation in quartz fibres at the brittle–ductile transition. Tectonophysics 303, 83–107.

Voll, G., 1976. Recrystallization of quartz, biotite and feldspars from Erstfeld to the Leventina nappe, Swiss Alps, and its geological significance. Schweizerische Mineralogische und Petrographische Mitteilungen 56, 641–647.

Vollbrecht, A., Stipp, M., Olesen, N.Ø., 1999. Crystallographic orientation of microcracks in quartz and inferred deformation processes: a study on gneisses from the German Continental Deep Drilling Project (KTB). Tectonophysics 303, 279–297.

Werling, E., 1992. Tonale-, Pejo- und Judicarien-Linie: Kinematik, Mikrostrukturen und Metamorphose von Tektoniten aus räumlich interferierenden aber verschiedenaltrigen Verwerfungszonen. Ph.D. Thesis, ETH Zürich.

White, S.H., 1973. Syntectonic recrystallisation and texture development in quartz. Nature 244, 276–277.

White, S.H., 1976. The effects of strain on the microstructures, fabrics and deformation mechanisms in quartz. Philosophical Transactions of the Royal Society of London A 283, 69–86.

White, S., 1977. Geological significance of recovery and recrystallization processes in quartz. Tectonophysics 39, 143–170.

White, S., 1979. Grain and sub-grain size variations across a mylonite zone. Contributions to Mineralogy and Petrology 70, 193–202.

Winkler, H.G.F., 1979. Petrogenesis of Metamorphic Rocks. Springer, New York 348pp.

Yardley, B.W.D., 1989. An Introduction to Metamorphic Petrology. , Earth Sciences Series. Longman 248pp.

Zulauf, G., 2001. Structural style, deformation mechanisms and paleodifferential stress along an exposed crustal section; constraints on the rheology of quartzofeldspathic rocks at supra- and infrastructural levels (Bohemian Massif). Tectonophysics 332, 211–237.